respectively. After IL-1β stimulation, the average ± SE of PGE_2 production in $FHIT^+$ cells and $FHIT^-$ cells was 187.17 ± 82.094 and 228.16 ± 103.74, respectively. With respect to the most appropriate COX-2 inducer, stimulation by LPS showed the largest difference between FHIT-expressing cells and FHIT-nonexpressing cells (Fig. 2*B*; $P < 0.018$).

Overexpression of FHIT suppresses PGE_2-stimulated cell proliferation. As shown in Fig. 2*C* (*left*), proliferation of both $FHIT^+$ and $FHIT^-$ cells increased in response to LPS stimulation. The most notable difference was observed at 96 hours after addition of a stimulator. At this time point, the average absorbance value obtained in 12 experimental data points between $FHIT^+$ and $FHIT^-$ cells was 1.244 ± 0.046 and 1.487 ± 0.056, respectively ($P = 0.0027$). At earlier times, the difference did not reach statistical significance; however, cell proliferation was generally lower in $FHIT^+$ cells than in $FHIT^-$ cells. In addition, it is notable that the difference in PGE_2 was remarkable between the two LPS-stimulated cells and the two non–LPS-stimulated cells in spite of FHIT status. We therefore concluded that cancer cells were affected by inflammatory stimulation. However, the difference was clearly observed in response level between $FHIT^+$ and $FHIT^-$ expression in LPS^+ cells.

We added ponasterone A every 24 hours to maintain continuous expression of FHIT protein. According to Western blotting analysis (Fig. 2*C*, *right*), COX-2 expression followed by PGE_2 activation was activated by LPS stimulant, which was independent from FHIT expression. In addition, we confirmed that FHIT expression was not directly affected by LPS stimulation; therefore, we concluded that the difference in cell proliferation between $FHIT^+$ and $FHIT^-$ cells under LPS stimulation lies in the influence of LPS on PGE_2 synthesis.

FHIT-knockdown colorectal cancer cells show an up-regulation of PGE_2 synthesis. We used DLD-1 and CCK-81 as FHIT mRNA-expressing colorectal cancer cell lines to be treated with *FHIT* siRNA as assessed by real-time RT-PCR (Fig. 3*A*). Fluorescence staining of FHIT protein in CCK-81 as well as DLD-1 was reduced by *FHIT* siRNA treatment (Fig. 3*B*), and expression of FHIT protein in siRNA-treated CCK-81 cells was suppressed to 24% of the level seen in parent FHIT-expressing cells, as assessed by Western blotting analysis (Fig. 3*C*).

As shown in Fig. 4*A*, production of PGE_2 was remarkably different between $FHIT^+$ control colorectal cancer cells and $FHIT^-$ siRNA-treated colorectal cancer cells. Especially in CCK-81 cells, synthesis of PGE_2 was inhibited under FHIT expression until 96 hours, whereas it was distinctively activated from 24 to 96 hours by LPS stimulation, with statistical significance by Student's *t* test ($P < 0.05$). Although the DLD-1 line had relatively higher production of PGE_2 in $FHIT^-$ siRNA-treated cells than in $FHIT^+$ control cells, there was no statistical significance between them.

FHIT-knockdown colorectal cancer cells proliferate with PGE_2 stimulation. As shown in Fig. 4*B*, the proliferation rate of CCK-81 cells was remarkably higher in FHIT-knockdown cells than in FHIT-expressing control cells, achieving statistical significance ($P < 0.05$) at 24, 48, 72, and 96 hours. On the other hand, DLD-1 showed no statistical significance in proliferation rates, but the cell proliferation rate in FHIT-knockdown cells was more than that in $FHIT^+$ DLD-1 cells. The CCK-81 line showed a much larger

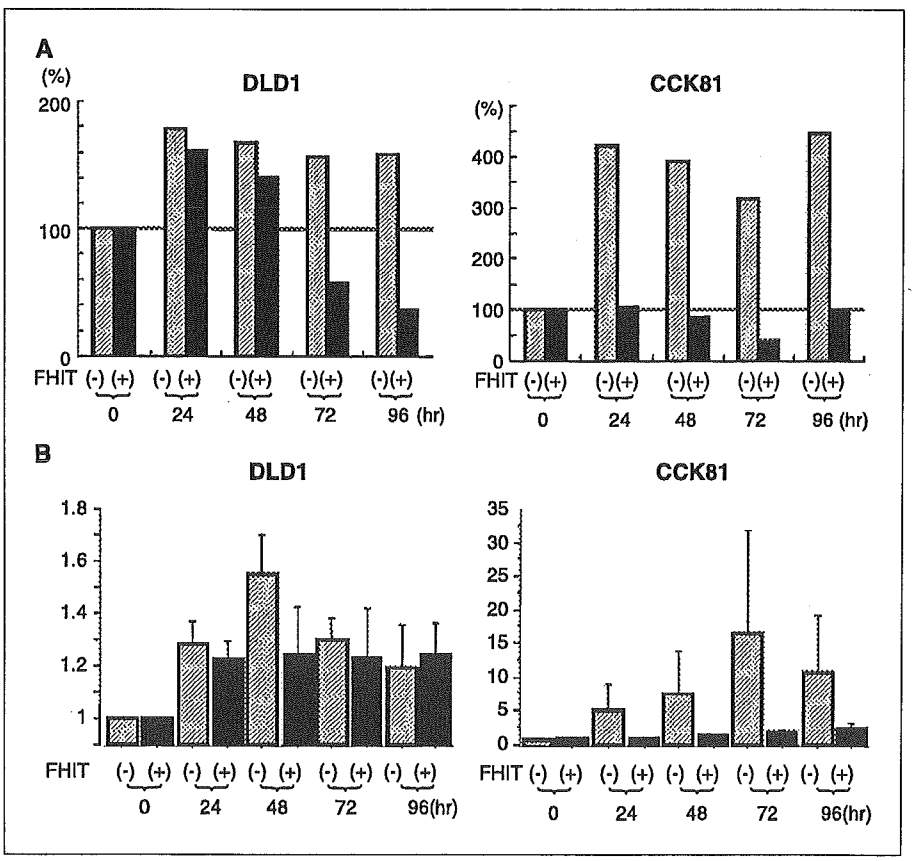

Figure 4. PGE_2 production and cell proliferation of FHIT knock-down colorectal cancer cells. FHIT siRNA knock-down vector was transfected to DLD1 and CCK81 cells; after confirming reduced expression, PGE_2 production assay was evaluated by ELISA (*A*) and MTT cell proliferation assay (*B*). Amount of PGE_2 production was evaluated in FHIT siRNA knock-down cells (*hatched column*) and mock-treated cells (*black column*) after exposure to LPS for indicated time. *Y-axis*, relative ratios (%) of PGE_2 production at 24, 48, 72, and 96 hours compared with production at time 0 in each cell. *X-axis*, elapsed time after LPS stimulation (1.0 μg/mL). Statistical significance was found for PGE_2 production between FHIT siRNA knock-down cells and mock-treated cells at 24, 48, 72, and 96 hours ($P < 0.017$). *B*, MTT assay. The experiment was done similarly to A. Y axis shows relative ratio of mean absorbance at 24, 48, 72, and 96 hours compared with cell proliferation at time 0 in each cell. Statistical significance was observed in mean absorbance in CCK-81 cell line between FHIT siRNA knock-down cells and mock-treated cells at 24, 48, 72, and 96 hours ($P < 0.05$).

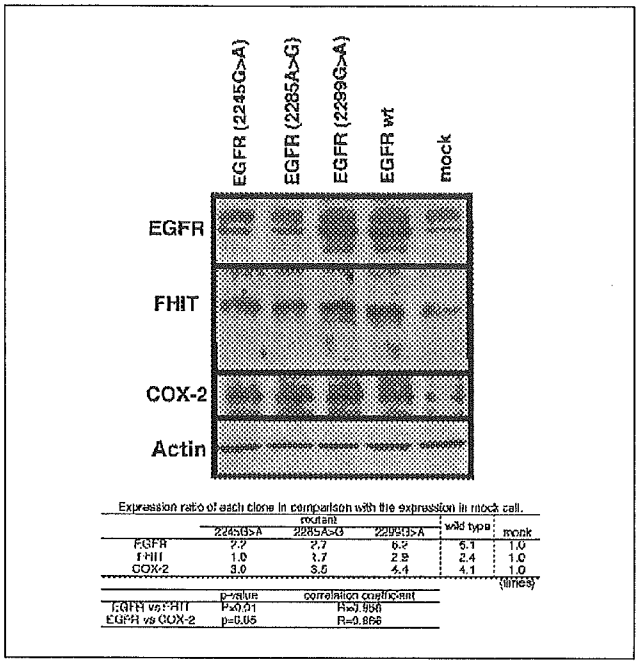

Figure 5. Association of induced EGFR expression with COX-2 and FHIT expression. Wild-type and mutant EGFR cDNA vectors were transfected and subjected to Western blot for assessment of COX-2 and FHIT expression. Up-regulation of both COX-2 and FHIT expression in EGFR cDNA transfected colorectal cancer cells was observed without LPS stimulation. Actin expression indicates an equal amount of protein loaded. *Bottom*, relative ratios of each expression. Wild-type and 2299/A767T mutant showed higher EGFR expression compared with other samples, concordant with increased expression of FHIT and COX-2.

difference between $FHIT^+$ and $FHIT^-$ cells than the DLD-1 line did in both ELISA assay and MTT assay.

Expression of FHIT is activated by abundant expression of EGFR. Figure 5 (*bottom*) shows expression ratios in each clone, such as wild type, and in three mutants compared with expression in mock cells. A significant association was observed between EGFR expression and FHIT expression (P = 0.01, R = 0.958). EGFR expression and COX-2 expression also showed concordance with each other; this finding has already been reported by Moraitis et al. (17).

Discussion

Immunohistochemical study showed a significant relationship between FHIT and COX-2 expression in colorectal cancer tumor samples; there was a tendency toward positive COX-2 expression in $FHIT^+$ tumors and vice versa. Our previous study of colorectal cancer reported that $FHIT^-$ tumors showed more aggressive biological behavior than $FHIT^+$ tumors. Expression status of COX-2 has also been reported to correlate with aggressive colorectal cancer behavior (21). Taken together, colorectal cancer tumors with $COX\text{-}2^+$ and $FHIT^-$ expression may be considered the most aggressive compared with the other three expression combination groups. Indeed, as shown in Table 1, deeper invasion was more frequently seen in $COX\text{-}2^+$, $FHIT^-$ tumors than tumors with the other three expression combinations.

As mentioned above, there was a significant association between FHIT and COX-2 expression when studied with immunohistochemistry. In contrast, there was no direct interaction between FHIT and COX-2 proteins in *in vitro* study (Fig. 2*A*). We then focused on PGE_2 because COX-2 is not thought to be directly associated with carcinogenesis; however, PGE_2 is intimately involved in carcinogenesis and in cancer biology (22). PGE_2 plays a main role in tumor cell proliferation through activation of molecules and pathways, such as EGFR, extracellular signal-regulated kinase 2 (23), and phosphatidylinositol 3-kinase signal pathways (24, 25). Moreover, PGE_2 is related to inhibition of apoptosis (26), activation of angiogenesis (27), and promotion of invasion or metastasis (28).

In the current study, PGE_2 production was significantly inhibited in enforced FHIT-expressing cells compared with vector-only transfectant ($FHIT^-$) cells. Cellular proliferation of both $FHIT^+$ and $FHIT^-$ cells increased in response to inflammatory stimulation. However, $FHIT^+$ cells showed reduced cell biology. On the other hand, FHIT-knockdown colorectal cancer cells showed increased production of PGE_2 as well as increased cell proliferation rate.

Given concordant expression between FHIT and COX-2 using immunohistochemical study, we focused on EGFR as the common upstream molecule. Moraitis et al. have reported that tobacco smoke activates *EGFR* expression in oral mucosa, and that its signal contributes to elevated levels of COX-2 (17). In addition, Dannenberg et al. have described a relationship among EGFR, COX-2, and carcinogenesis (29). In the current study, as shown in Fig. 2, induction of COX-2 was affected by LPS stimulation but not by FHIT. Moreover, Fig. 5 shows concordant expression of FHIT protein and COX-2 protein along with various expression levels of EGFR protein in wild-type and/or mutant-type clones in the absence of LPS inflammatory stimulation. Therefore, we conclude that COX-2 and FHIT were elevated by EGFR expression as one of the common upstream molecules. However, it is not known how FHIT is activated by EGFR, a receptor-type tyrosine kinase.

Considering together the inverse correlation between FHIT and PGE_2 and the positive association between FHIT and COX-2, we speculated that in colorectal cancer subjected to inflammatory stimulation, COX-2 expression is associated with abundant FHIT expression. In endogenously $FHIT^+$ colorectal cancer tumors, PGE_2 production was suppressed, which led to regulation or quenching, if any, of cell proliferation activity downstream. However, $FHIT^-$ colorectal cancer, presumably due to genetic and epigenetic alterations, may have lost physiologic regulation of PGE_2 production, which would contribute to malignant cellular behavior. FHIT is supposed to function as a tumor suppressor, at least partially via regulation of PGE_2 production, even in a $COX\text{-}2^+$ background.

In conclusion, an analysis of FHIT and COX-2 expression in colorectal cancer tumors would be helpful to clinicians by indicating malignant potential. One could select patients with altered FHIT expression as candidates for treatment with COX-2 inhibitors aimed at prevention of cancer progression. Moreover, abundant expression of FHIT protein should have a role as a cancer suppressor against inflammation-mediated carcinogens that are mainly regulated by PGE_2.

Acknowledgments

Received 7/21/2005; revised 12/6/2005; accepted 12/16/2005.

Grant support: Core Research for Evolutional Science and Technology; Japan Science and Technology Agency, Japan Society for the Promotion of Science grants-in-aid for Scientific Research; and grants 17109013, 17591411, 17591413, 17015032, and 16390381.

The costs of publication of this article were defrayed in part by the payment of page charges. This article must therefore be hereby marked *advertisement* in accordance with 18 U.S.C. Section 1734 solely to indicate this fact.

We thank Dr. Jennifer Pietenpol for the generous gift of H1299 stably transfected with the pVgRXR vector and for the pIND vector, Dr. A. Takayanagi for providing the EGFR vector, and Shimo-oka and Mrs. Nagahara for their valuable technical support.

References

1. Huebner K, Croce CM. FRA3B and other common fragile sites: the weakest links. Nat Rev Cancer 2001;1: 214–21.
2. Inoue H, Ishii H, Alder H, et al. Sequence of the FRA3B common fragile region: implications for the mechanism of FHIT deletion. Proc Natl Acad Sci U S A 1997;94: 14584–9.
3. Ishii H, Mimori K, Inageta T, et al. Components of DNA damage checkpoint pathway regulate UV exposure-dependent alterations of gene expression of FHIT and WWOX at chromosome fragile sites. Mol Cancer Res 2005;3:130–8.
4. Mimori K, Druck T, Inoue H, et al. Cancer-specific chromosome alterations in the constitutive fragile region FRA3B. Proc Natl Acad Sci U S A 1999;96: 7456–61.
5. Mori M, Mimori K, Masuda T, et al. Absence of Msh2 protein expression is associated with alteration in the FHIT locus and FHIT protein expression in colorectal carcinoma. Cancer Res 2001;61:7379–82.
6. Nelson HH, Wiencke JK, Gunn L, Wain JC, Christiani DC, Kelsey KT. Chromosome 3p14 alterations in lung cancer: evidence that FHIT exon deletion is a target of tobacco carcinogens and asbestos. Cancer Res 1998;58: 1804–7.
7. Sozzi G, Sard L, De Gregorio L, et al. Association between cigarette smoking and FHIT gene alterations in lung cancer. Cancer Res 1997;57:2121–3.
8. Sozzi G, Pastorino U, Moiraghi L, et al. Loss of FHIT function in lung cancer and preinvasive bronchial lesions. Cancer Res 1998;58:5032–7.
9. Stein CK, Glover TW, Palmer JL, Glisson BS. Direct correlation between FRA3B expression and cigarette smoking. Genes Chromosomes Cancer 2002;34:333–40.
10. Tseng JE, Kemp BL, Khuri FR, et al. Loss of Fhit is frequent in stage I non-small cell lung cancer and in the lungs of chronic smokers. Cancer Res 1999;59: 4798–803.
11. Mori M, Mimori K, Shiraishi T, et al. Altered expression of Fhit in carcinoma and precarcinomatous lesions of the esophagus. Cancer Res 2000;60:1177–82.
12. Ishii H, Ozawa K, Furukawa Y. Alteration of the fragile histidine triad gene early in carcinogenesis: an update. J Exp Ther Oncol 2003;3:291–6.
13. Ishii H, Dumon KR, Vecchione A, et al. Potential cancer therapy with the fragile histidine triad gene: review of the preclinical studies. JAMA 2001;286:2441–9.
14. Ishii H, Dumon KR, Vecchione A, et al. Effect of adenoviral transduction of the fragile histidine triad gene into esophageal cancer cells. Cancer Res 2001;61: 1578–84.
15. Woods JM, Mogollon A, Amin MA, Martinez RJ, Koch AE. The role of COX-2 in angiogenesis and rheumatoid arthritis. Exp Mol Pathol 2003;74:282–90.
16. Druck T, Hadaczek P, Fu TB, et al. Structure and expression of the human FHIT gene in normal and tumor cells. Cancer Res 1997;57:504–12.
17. Moraitis D, Du B, De Lorenzo MS, et al. Levels of cyclooxygenase-2 are increased in the oral mucosa of smokers: evidence for the role of epidermal growth factor receptor and its ligands. Cancer Res 2005;65: 664–70.
18. Livneh E, Prywes R, Kashles O, et al. Reconstitution of human epidermal growth factor receptors and its deletion mutants in cultured hamster cells. J Biol Chem 1986;261:12490–7.
19. Nagahara H, Mimori K, Ohta M, et al. Somatic mutations of epidermal growth factor receptor in colorectal carcinoma. Clin Cancer Res 2005;11:1368–71.
20. Eberhart CE, Coffey RJ, Radhika A, Giardiello FM, Ferrenbach S, DuBois RN. Up-regulation of cyclooxygenase 2 gene expression in human colorectal adenomas and adenocarcinomas. Gastroenterology 1994;107:1183–8.
21. Soumaoro LT, Uetake H, Higuchi T, Takagi Y, Enomoto M, Sugihara K. Cyclooxygenase-2 expression: a significant prognostic indicator for patients with colorectal cancer. Clin Cancer Res 2004;10:8465–71.
22. Baratelli F, Lin Y, Zhu L, et al. Prostaglandin E2 induces FOXP3 gene expression and T regulatory cell function in human $CD4^+$ T cells. J Immunol 2005;175:1483–90.
23. Pai R, Soreghan B, Szabo IL, Pavelka M, Baatar D, Tarnawski AS. Prostaglandin E_2 transactivates EGF receptor: a novel mechanism for promoting colon cancer growth and gastrointestinal hypertrophy. Nat Med 2002; 8:289–93.
24. Buchanan FG, Wang D, Bargiacchi F, DuBois RN. Prostaglandin E_2 regulates cell migration via the intracellular activation of the epidermal growth factor receptor. J Biol Chem 2003;278:35451–7.
25. Leng J, Han C, Demetris AJ, Michalopoulos GK, Wu T. Cyclooxygenase-2 promotes hepatocellular carcinoma cell growth through Akt activation: evidence for Akt inhibition in celecoxib-induced apoptosis. Hepatology 2003;38:756–68.
26. Tsujii M, DuBois RN. Alterations in cellular adhesion and apoptosis in epithelial cells overexpressing prostaglandin endoperoxide synthase 2. Cell 1995;83:493–501.
27. Tsujii M, Kawano S, Tsuji S, Sawaoka H, Hori M, DuBois RN. Cyclooxygenase regulates angiogenesis induced by colon cancer cells. Cell 1998;93:705–16.
28. Tsujii M, Kawano S, DuBois RN. Cyclooxygenase-2 expression in human colon cancer cells increases metastatic potential. Proc Natl Acad Sci U S A 1997;94: 3336–40.
29. Dannenberg AJ, Lippman SM, Mann JR, Subbaramaiah K, DuBois RN. Cyclooxygenase-2 and epidermal growth factor receptor: pharmacologic targets for chemoprevention. J Clin Oncol 2005;23:254–66.

Specific Peptide Ligand for Grb7 Signal Transduction Protein and Pancreatic Cancer Metastasis

Shinji Tanaka, Stephanie C. Pero, Kenichi Taguchi, Mitsuo Shimada, Masaki Mori, David N. Krag, Shigeki Arii

Background: **Pancreatic cancer is one of the most aggressive malignancies, with high rates of invasion and metastasis and with generally poor prognosis. We previously found that metastasis was strongly associated with the expression of growth factor receptor–bound protein 7 (Grb7), which contains a Src homology 2 (SH2) domain. In this study, we evaluated Grb7 protein as a molecular target of therapy for metastatic pancreatic cancer.** ***Methods:*** **Grb7 protein expression was measured by immunohistochemistry in 36 human pancreatic cancer specimens and adjacent normal pancreatic tissue. We synthesized a nonphosphorylated peptide inhibitor that binds specifically to the SH2 domain of Grb7. Intracellular signaling was assessed by immunoprecipitation and immunoblot assays in cultured human pancreatic cancer cells. Cell migration was measured with a modified Boyden chamber method. Peritoneal metastasis of the pancreatic cancer cells was measured with a mouse model. All statistical tests were two-sided.** ***Results:*** **We found that 22 (61%) of 36 pancreatic cancer specimens had higher levels of Grb7 protein than their corresponding normal pancreatic tissue specimens. Grb7 expression was statistically significantly different between specimens from patients without lymph node metastasis (stage N0; two of the 10 patients) and patients with lymph node metastasis (stages N1 + N2; 20 of the 26 patients) ($P = .006$). The Grb7 peptide inhibitor selectively blocked the interaction between Grb7 and focal adhesion kinase and blocked the phosphorylation of Grb7 protein. In vivo Grb7 peptide inhibitor statistically significantly attenuated cell migration (for control peptide, 87.5 cells migrated, 95% confidence interval [CI] = 82.6 to 92.4 cells; for Grb7 peptide, 5.7 cells migrated, 95% CI = 2.3 to 9.0 cells; $P<.001$, t test) and peritoneal metastasis of the pancreatic cancer cells in a mouse model, as assessed by the number of nodules (control = 72.6 nodules, 95% CI = 55.8 to 89.4 nodules; and for Grb7 peptide = 3.2 nodules, 95% CI = 1.6 to 4.8 nodules; $P<.001$, t test) and their weight (control = 4.13 g, 95% CI = 3.40 to 4.86 g; Grb7 peptide = 0.19 g, 95% CI = 0.06 to 0.32 g; $P<.001$, t test).** ***Conclusions:*** **The Grb7 peptide inhibitor appears to be a promising molecularly targeted therapeutic agent against metastatic pancreatic cancer. [J Natl Cancer Inst 2006;98:491–8]**

Pancreatic cancer, which is among the most aggressive of all human malignancies, has a 5-year survival rate of less than 1% *(1,2)*. It is the fourth leading cause of cancer death in the United States and the fifth leading cause of cancer death in Japan, and the cause-specific death rate of the pancreatic cancer is gradually increasing worldwide *(1)*. Invasion and metastasis of tumor cells are major risk factors that decrease the clinical prognosis of patients with pancreatic cancer. The mechanism for invasion and metastasis involves the activation of members of the protein tyrosine kinase family, followed by the transmission of intracellular signals *(3)*. The subsequent tyrosyl phosphorylation of intracellular substrates leads to their interaction with Src homology 2 (SH2) domains of downstream signaling molecules *(4)*. Because of the specific role of the SH2 domains in signal transduction pathways, SH2-mediated protein–protein interactions are attractive therapeutic targets for cancer treatment *(5)*.

We have previously identified Grb7, an SH2-containing adaptor protein that is frequently overexpressed in invasive and metastatic human cancer tissues *(6)*. The predicted protein structure of Grb7 shares structural homology with Mig-10, a cell migration molecule from *Caenorhabditis elegans*, that is required for embryonic cell migration to the neural cleft *(7,8)*. It is noteworthy that the human Grb7 gene is located at chromosomal position 17q12-q22 within an amplicon of the erbB2 gene, which is frequently amplified in various cancer cells *(9,10)*. The Grb7 protein can bind to various protein tyrosine kinases, including members of the erbB family *(10–12)* and focal adhesion kinase (FAK) *(13)*, whose activities play critical roles in cell migration *(14,15)*. Therefore, competitive targeting of interactions involving the SH2 domain of Grb7 protein might affect the migration of human cancer cells *(16–18)*. Although specific phosphotyrosine-containing peptides with a minimal recognition motif can compete in vitro with phosphorylated protein ligands for SH2 domain binding, these peptides are less able to compete in vivo because the various phosphatases that are present in tissues inactivate these peptides by removing the phosphate groups. This problem prompted us to develop inhibitors that do not require phosphate groups to target SH2 domains, such as the nonphosphorylated cyclic peptides with selective affinity to SH2 domains that we previously developed by use of phage-display technology *(19)*. One of these peptides, termed G7-18NATE, binds specifically to the SH2 domain of Grb7 protein and inhibits the binding of Grb7 protein to various protein tyrosine kinases *(20)*.

In the study, we analyzed Grb7 protein expression in human pancreatic cancer tissue specimens to determine whether it was associated with the metastatic spread of pancreatic cancer and

Affiliations of authors: Department of Hepato-Biliary-Pancreatic Surgery, Graduate School of Medicine, Tokyo Medical and Dental University, Tokyo, Japan (ST, SA); Department of Surgery, University of Vermont School of Medicine, Burlington, VT (SCP, DNK); Institute of Clinical Research, National Kyushu Cancer Center, Fukuoka, Japan (KT); Department of Digestive and Pediatric Surgery, Institute of Health Bioscience, University of Tokushima Graduate School, Tokushima, Japan (MS); Department of Molecular and Surgical Oncology, Medical Institute of Bioregulation, Kyushu University, Beppu, Japan (MM).

Correspondence to: Shinji Tanaka, MD, PhD, Department of Hepato-Biliary-Pancreatic Surgery, Graduate School of Medicine, Tokyo Medical and Dental University, 1-5-45 Yushima, Bunkyo-ku, Tokyo 113-8519, Japan (e-mail: shinji.msrg@tmd.ac.jp).

See "Notes" following "References."

DOI: 10.1093/jnci/djj105

could be a molecular target for metastatic pancreatic cancer therapy. We attached a penetratin sequence to the Grb7 peptide inhibitor G7-18NATE, resulting in G7-18NATE-P, to facilitate its uptake by cells *(21)*. We also evaluated the in vivo effects of the Grb7 peptide inhibitor on cell migration and peritoneal metastasis of the pancreatic cancer cells.

Materials and Methods

Tissue Specimens

We studied 36 specimens (23 from men and 13 from women; mean age = 65.2 years) of primary pancreas adenocarcinomas for Grb7 expression, as described previously *(7)*. Written informed consent from these patients and institutional review board approval were obtained. Pancreatic cancer tissues were fixed with periodate–lysine–paraformaldehyde at 4 °C, embedded in OCT compound, and stored at −80 °C. Sections that were 4 μm thick were cut and then stained with hematoxylin–eosin for histopathologic analysis.

Immunohistochemistry

We used immunohistochemistry to evaluate the expression of Grb7 protein in sections of human pancreatic cancer tissue *(7,22)*. The anti-Grb7 polyclonal antibody (product C-20; Santa Cruz Biochemistry, Santa Cruz, CA) was used at 1 : 50 dilution in phosphate-buffered saline (PBS) containing 1% bovine serum albumin (Sigma Chemical, St. Louis, MO), followed by incubation for 6 hours at room temperature. Antibody binding was then immunodetected with the avidin–biotin–peroxidase complex, as described by the supplier (Nichirei, Tokyo, Japan). Sections were lightly counterstained with hematoxylin to stain the nucleus. Grb7-positive staining of cancer cells was determined by comparison with the Grb7-negative staining of adjacent normal acinar and duct cells, the internal negative control. Immunohistochemical staining was evaluated under a light microscope by three independent pathologists (K. Taguchi, M. Mori, and S. Arii). Cancer tissue specimens were scored as positive if more than 20% of the tumor cells stained positive for Grb7; specimens were scored as negative if less than 20% tumor cells were positive for Grb7.

Immunoblot Analysis

Pancreatic tissues or cells were prepared for immunoblot analysis as described *(7,22)*. Fixed tissues or cells were lysed in ice-cold Triton buffer (50 mM Tris-HCl at pH 7.5, containing 1% Triton X-100, 2 mM EGTA, 10 mM EDTA, 100 mM NaF, 1 mM $Na_4P_2O_7$, 2 mM $NaVO_4$, 1 mM phenylmethylsulfonyl fluoride, aprotinin at 25 mg/mL, pepstatin A at 3.5 mg/mL, and leupeptin at 25 mg/mL), followed by centrifugation at 14 000*g* for 15 minutes at 4 °C. Next, 50 μg of the supernatant per lane was subjected to electrophoresis through sodium dodecyl sulfate–polyacrylamide gels and transferred onto Immobilon-P membranes (Millipore Corp., Bedford, MA). Blots were incubated for 6 hours at 4 °C with specific antibody, and bands were detected via the ECL system (Amersham, Arlington Heights, IL). For immunoprecipitation analysis, the lysate supernatant containing 500 μg of protein was incubated with 10 μg of antibody and precipitated with protein A–agarose for 6 hours at 4 °C. We used anti-Grb7 polyclonal antibody (product sc-606; Santa Cruz Biotechnology, Santa Cruz, CA), anti-Grb2 monoclonal antibody (product sc-8034; Santa Cruz Biotechnology), anti-Grb10 polyclonal antibody (product sc-13955; Santa Cruz Biotechnology), anti-phosphotyrosine monoclonal antibody conjugated to horseradish peroxidase (product PY20H; Transduction Laboratories. Lexington, KY), and anti-FAK monoclonal antibody (clone 77; Transduction Laboratories) and anti–epidermal growth factor receptor (EGFR) monoclonal antibody (clone 77; Oncogene Research Products, Cambridge, MA). All antibodies were used at a 1:200 dilution, except for PY20H, which was used at a 1:1000 dilution. As secondary antibodies, horseradish peroxidase–conjugated anti-mouse immunoglobulin G (IgG) antibody and anti-rabbit IgG antibody were used at 1:10000 dilutions (products NA931 and NA934; Amersham).

Real-Time Quantitative Genomic Polymerase Chain Reaction Analysis

Pancreatic tissue preparation, microdissection of pure tumor cell populations from fixed tissue, and nucleic acid extraction from paraformaldehyde-fixed tissues for polymerases chain reaction (PCR) analysis were carried out as described in our previous report *(6)*. Amplification of Grb7 and erbB2 sequences was carried out by real-time PCR with the ABI PRISM 7700 Sequence Detection System (Applied Biosystems, Foster City, CA), as described by Walch et al. *(23)*. The following primers and probes were prepared to amplify genomic erbB2 sequences (sense, 5′CA GAAGGTCTACATGGGTGCTTC-3′; antisense, 5′-TTCCGAGC GGCCAAGTC-3′; probe, 5′-TGGAGGATGTGCGGCTCGTAC ACA-3′), Grb7 sequences (sense, 5′-CAAGTCCTGCTCACTCA TGCTG-3′; antisense, 5′-ACGTTGGACTCGTTCACATCTG-3′; probe, 5′-AGGATCCGAGGCACCTGCAGTACGTG-3′), and globin sequences (sense, 5′-ACCCTTAGGCTGCTGGTGG-3′; antisense, 5′-GGAGTGGACAGATCCCCAAA-3′; probe, 5′-CTA CCCTTGGACCCAGAGGTTCTTTGAGTC-3′). Copy numbers of Grb7, erbB2, and globin genes per cell were calculated by linear regression analysis from an external standard curve generated from pooled genomic DNA from human blood cells. Cut points for altered Grb7 and erbB2 copy numbers were defined by the mean value of the Grb7/globin and erbB2/globin expression ratios determined in normal pancreatic tissues plus four standard deviations. Cut points were 5.17-fold for Grb7 and 5.05-fold for erbB2.

Synthesis of Small Interfering RNA and Peptides

The targeted sequence for human Grb7 small interfering RNA (siRNA) (5′-AACGAGUCCAACGUGUACGUG-3′) was designed as described *(24)*. The siRNA was synthesized and labeled with Alexa Fluor 488 by QIAGEN Inc. (Hilden, Germany). The negative control siRNA, labeled with Alexa Fluor 488 (5′-AA UUCUCCGAACGUGUCACGU-3′; product 1022563), was purchased from QIAGEN. Thioether-cyclized peptides were synthesized by Bio-Synthesis Inc. (Lewisville, TX), as previously described *(20)*. Briefly, the peptides were synthesized on a Rink Amide resin (product 01-64-0013; Novabiochem) by standard solid-phase synthesis with fluorenylmethoxycarbonyl (Fmoc) chemistry *(25)*. *N-a*-Fmoc-*S-p*-methoxytrityl-L-cysteine [Fmoc-cys(Mmt)-OH] (04-12-1061; Novabiochem) was used in this synthesis. After attaching the amino acids and bromoacetylating the amino-terminal peptide, the protected cysteine side chain was deprotected with 1% trifluoroacetic acid (TFA) in CH_2Cl_2, and then the peptide was cyclized in 1% *N,N*-diisopropylethylamine

in dimethylformamide for 24 hours. The cyclic peptide was cleaved from the support under standard conditions (5% 2-{[2-hydroxy-1, 1-bis(hydroxymethyl)ethyl]amino}ethanesulfonic acid–95% TFA). The peptides were purified by reverse-phase high-pressure liquid chromatography on a Phenomenex Jupiter C_{18} column (solution A = 0.5% TFA in water; solution B = 0.5% TFA in acetonitrile) gradient = solution A to solution B over 40 minutes). To improve the uptake of the Grb7 peptide inhibitor G7-18NATE by cells for in vivo studies, we covalently attached a penetratin peptide *(21)* to G7-18NATE to produce G7-18NATE-P (WFEGYDN TFPC-RQIKIWFQNRRMKWKK). As a control, we used the penetratin peptide without an attached peptide (RQIKIWFQNR RMKWKK).

Cell Culture, Transfection, Proliferation, and Migration Assays

Human pancreatic cancer cell lines, Panc-1, MiaPaca2, PK8, and KLM1, were cultured in RPMI 1640 medium (Sigma) supplemented with 10% heat-inactivated fetal bovine serum (Sigma). Multichannel confocal laser–scanning microscopy was used for analysis of the living cell cultures. Panc-1 cells were transfected with siRNA oligonucleotides by use of Lipofectamine 2000 Reagent (GIBCO BRL, Life Technologies, Inc., Gaithersburg, MD) essentially as described elsewhere *(7)*, except that we used 60% confluent cells.

Assays of cell proliferation and migration were performed as described previously *(7,22)*. For proliferation assays, 1×10^5 cells were cultured on 10-cm plastic dishes, and the number of cells was counted every other day for 8 days. For migration assays, we used a modified Boyden chamber and 24-well plates containing polyethylene terephthalate filter inserts (8-μm pores) that were coated with fibronectin (Collaborative Biomedical Products, Bedford, MA). First, 1×10^4 cells were suspended in serum-free medium containing 0.5% bovine serum albumin and placed in the upper chamber, and then the lower chamber was filled with the same medium. After a 16-hour incubation, cells were fixed with 5% glutaraldehyde in PBS and stained with 0.5% trypan blue in 2% Na_2CO_3. Cells on the upper side of the filter were carefully removed with a cotton swab, and cells invading the lower side of the filter were counted by microscopic examination. The mean migration rate derived from three independent experiments was determined for each clone.

Mouse Model of Pancreatic Cancer Peritoneal Metastasis

To produce experimental tumor metastases *(26)*, we suspended 5×10^6 Panc-1, MiaPaca2, or KLM1 cells in 200 μL of RPMI 1640 medium and injected them intraperitoneally into BALB/c nu/nu mice at 5 weeks of age (mouse CAnN.Cg-*Foxn1*^{nu}/CrlCrlj; Charles River Japan, Inc., Yokohama, Japan). Mice were randomly assigned (five mice per group) to treatment with the Grb7 peptide inhibitor (10 mmol/kg) or the control peptide (10 mmol/kg); the peptides were injected intraperitoneally at the time of cell implantation and every third day for 2 weeks. On day 14, all mice were killed by cervical dislocation under anesthesia, macroscopic nodules on the peritoneal surface were counted and excised, and each nodule was weighed. Data presented are the means of three independent experiments.

To investigate whether the Grb7 peptide inhibitor had adverse side effects, we injected BALB/c nu/nu mice with the Grb7 peptide inhibitor at 1, 10, or 100 mmol/kg intraperitoneally every third day for 4 weeks and determined the body weight of the mice and any histologic changes of the major tissues, including liver, kidney, spleen, and lung. The growth of subcutaneously injected pancreatic tumor was also assessed as described previously *(27)*. All in vivo procedures were approved by the animal care committee of Tokyo Medical and Dental University.

Statistical Analysis

Statistical significance was assessed by a chi-square test or Fisher's exact test with a single degree of freedom. Two-sided Student's *t* tests (StatView software, Abacus Concepts, Inc., Berkeley, CA) were used to analyze differences between continuous values of two independent groups. *P* values of less than .05 were considered to have statistical significance. All statistical tests were two-sided.

Results

Grb7 Expression in Clinical Samples of Pancreatic Cancer

To determine whether Grb7 protein has clinical significance in human pancreatic cancer, we assessed the expression of Grb7 protein in human pancreatic cancer tissue specimens obtained from surgical resection by immunohistochemical analysis. We found that 22 (61%) of the 36 pancreatic cancer specimens examined had higher expression of Grb7 protein than the adjacent normal tissue, which had little if any expression in all 36 specimens (Fig. 1, A). We confirmed overexpression of Grb7 protein in some pancreatic cancers by Western blot analysis of tumor tissue lysates and also detected phosphorylation of Grb7 protein on tyrosine residues in tumors overexpressing Grb7 protein (Fig. 1, B).

The human Grb7 gene is located at chromosomal position 17q12-q22 within an amplicon of the erbB2 gene, which is frequently amplified in pancreatic cancer cells *(28)*. To determine whether the Grb7 and erbB2 genes were amplified in our tumor specimens, we used quantitative PCR, as described elsewhere *(23)*. We found that both Grb7 genes (median = 12.0 copies per cell, interquartile range = 8.9–23.3 copies per cell, and range = 7.2–36.2 copies per cell) and erbB2 genes (median = 14.8 copies per cell, interquartile range = 9.8–18.3 copies per cell, and range = 7.9–23.3 copies per cell) were amplified in 13 of the 22 tumors that overexpressed Grb7 protein, but we did not detect amplification of Grb7 or erbB2 genes in any of the tumors that did not overexpress Grb7 protein ($P<.001$; *t* test). Thus, overexpression of Grb7 protein might be associated with gene amplification of the 17q12-q22 chromosomal region in some pancreatic tumors.

Grb7 overexpression also appeared to be associated with lymph node status (Fig. 1, C). Among patients without lymph node metastases, Grb7 overexpression was observed in pancreatic cancer specimens from only two (20%) of the 10 patients. Among patients with regional lymph node metastases, Grb7 was overexpressed in pancreatic cancer specimens from 12 (67%) of the 18 patients with N1 stage disease and from all eight (100%) patients with N2 stage disease. Grb7 expression was statistically significantly different between specimens from patients without (stage N0; two of the 10 patients) and specimens from patients with

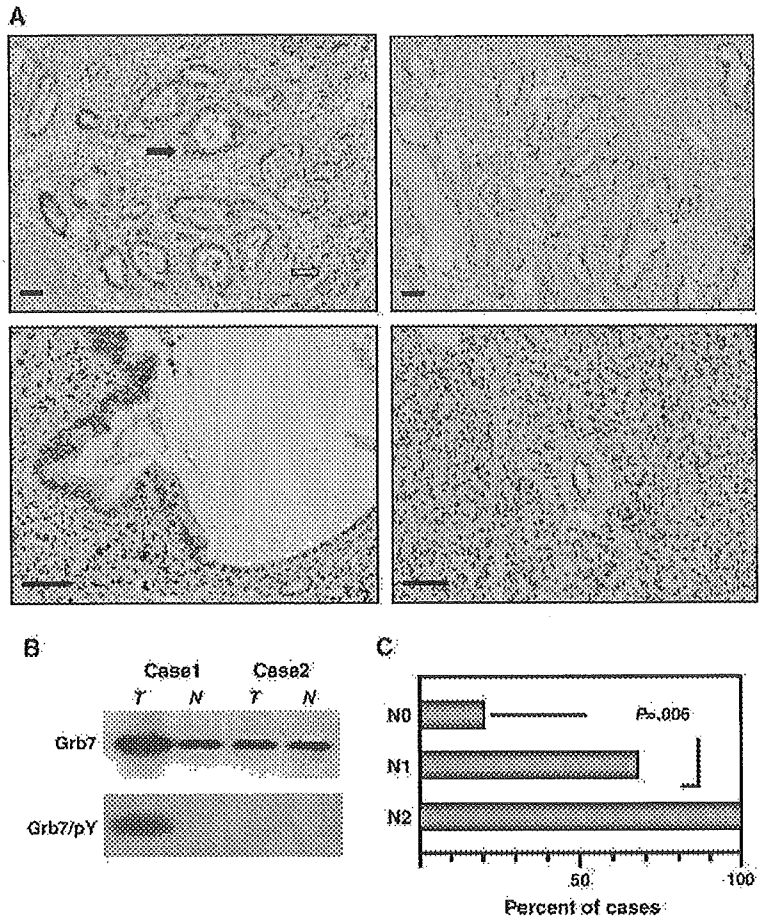

Fig. 1. Histologic analysis of Grb7 expression in human pancreatic cancer tissues. **A)** Immunohistochemistry. Representative examples of pancreatic cancer tissue and adjacent normal tissue are shown. Similar tissues gave similar results. Immunohistochemistry used an anti-Grb7 monoclonal antibody. **Left)** Positive staining for Grb7 protein in pancreatic cancer cells, compared with surrounding noncancer acinar and duct cells (original magnifications: upper = ×100, lower = ×200). Positive staining = **solid arrowheads**; negative staining = **open arrowheads**. **Right)** Lack of staining for Grb7 protein in pancreatic cancer cells (original magnifications: upper = ×100) or noncancer acinar and duct cells (original magnifications: lower = ×200). **Scale bars** = 100 μm. **B)** Immunoblot analysis. **Upper)** Expression of total Grb7. **Lower)** Expression of phosphorylated Grb7 (Grb7/pY). Expression was detected with an anti-Grb7 protein antibody C-20 and with an anti-phosphotyrosine antibody, respectively, in a lysate from pancreatic tumor tissue (**lanes T**) and a lysate from adjacent noncancerous tissue (**lanes N**). **Left)** Case 1, a Grb7-positive tumor. **Right)** Case 2, a Grb7-negative tumor. For the analysis of phosphorylated Grb7 protein, the lysate was first immunoprecipitated with the anti-Grb7 antibody and then the immunoprecipitated proteins were separated by electrophoresis and examined by immunoblot analysis. **C)** Grb7 expression and metastatic spread to lymph nodes of pancreatic cancer in 36 patients with pancreatic cancer. **Bars** = percentage of Grb7 overexpression in tumors with no metastasis (stage N0; bar N0), metastasis only to the regional lymph nodes (stage N1; bar N1), or metastasis to the distant lymph nodes (stage N2; bar N2). A two-sided Fisher's exact test was used to determine that the difference in Grb7 expression between tumors from patients without (N0) and with metastasis to lymph nodes (N1 + N2) was statistically significant ($P = .006$).

(stages N1 + N2; 20 of the 26 patients) lymph node metastasis ($P = .006$). Thus, increased expression of Grb7 protein appeared to be associated with regional lymph node metastatic spread of pancreatic cancer.

Inhibition of Grb7 Gene Expression with Grb7 siRNA in Human Pancreatic Cancer Cells

To explore the biological role of Grb7 overexpression in the cancer phenotype, we used knock-down analysis of Grb7 gene expression in human pancreatic cancer cells *(24)*. We transfected Grb7 siRNAs labeled with a fluorescent dye into Panc-1 human pancreatic cells (Fig. 2, A) and assessed the expression of Grb7 protein by immunoblotting with anti-Grb7 polyclonal antibody. We found that expression of Grb7 protein in cells transfected with Grb7 siRNA was lower than that in nontransfected cells and in cells transfected with control siRNA (Fig. 2, B).

We then used these transfected cells to investigate whether migration into fibronectin, as measured in a modified Boyden chamber *(22)*, was altered in cancer cells transfected with Grb7 siRNA. Grb7 siRNA tranfection reduced the migration of pancreatic cancer cells, compared with that nontransfected control cells or cells transfected with a control siRNA (control siRNA = 84.8 cells migrated; Grb7 siRNA = 20.7 cells migrated; difference = 64.2 cells migrated, 95% confidence interval [CI] = 47.3 to 81.1 cells migrated; $P<.001$; Fig. 2, C). As in our previous results with antisense Grb7 *(7)*, these results indicate that Grb7 overexpression plays a role in cancer cell migration.

Effect of Grb7 Peptide Inhibitor on Intracellular Signaling, Proliferation, and Migration of Human Pancreatic Cancer Cells

We have previously described the Grb7 peptide inhibitor G7-18NATE (Fig. 3, A), which binds specifically to the SH2 domain of Grb7 protein and inhibits the association of Grb7 protein with various members the protein tyrosine kinase family *(10)*. In this study, we used G7-18NATE-P (i.e., G7-18NATE to which we added a penetratin sequence to facilitate the intracellular uptake of the inhibitor). By use of multichannel confocal laser–scanning microscopy, we found that Panc-1 human pancreatic cancer cells can take up fluorescently labeled G7-18 NATE-P (Fig. 3, B).

In our previous studies, we found that Grb7 protein can interact with and phosphorylate FAK in fibronectin-stimulated cells *(22)*. To further assess intracellular Grb7 signaling, Panc-1 cells were stimulated with fibronectin, and the interaction of endogenous Grb7 protein with FAK and the phosphorylation of Grb7 protein on tyrosine residues were examined by immunoprecipitation with anti-FAK and anti-Grb7 antibodies. Both the interaction between Grb7 and FAK and the level of phosphorylated Grb7 were reduced after treatment with the Grb7 peptide inhibitor

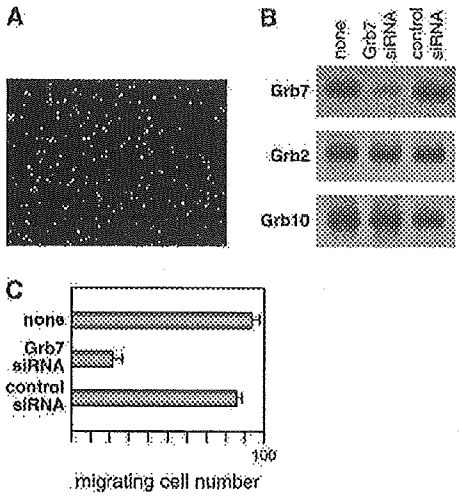

Fig. 2. RNA interference of Grb7 expression in human pancreatic cancer cells. **A)** Transfection of fluorescent-labeled siRNAs in the Panc-1 living human pancreas cancer cells. Fluorescently labeled siRNAs are shown as **green** on multichannel confocal laser–scanning microscopy. **B)** Expression of Grb family proteins in fibronectin-stimulated Panc-1 cells transfected with Grb7 siRNA or with control siRNA or nontransfected control Panc-1 cells (none). **C)** Fibronectin migration assay. The number of cells migrating into the fibronectin was determined for Panc-1 cells transfected with Grb7 siRNA or with control siRNA or nontransfected control Panc-1 cells (none) with a modified Boyden chamber method. The mean migration rate, expressed as cell numbers, derived from three independent experiments for duplicates per point (control siRNA = 84.8 cells and Grb7 siRNA = 20.7 cells; difference = 64.2 cells, 95% confidence interval = 47.3 to 81.1 cells; $P<.001$). All statistical tests were two-sided.

G7-18NATE-P (Fig. 3, C). To investigate the specificity of the Grb7 peptide inhibitor for these activities, we repeated the experiments but assessed Grb2 and Grb10, other endogenous SH2-containing proteins. We found that G7-18NATE-P did not affect the interaction of Grb2 with FAK or with EGFR (Fig. 3, C) and that the peptide inhibitor did not affect tyrosyl phosphorylation of Grb10 (Fig. 3, C). The proliferation of pancreatic cells treated with the Grb7 peptide inhibitor was not statistically significantly different from that of untreated cells (Fig. 3, D).

To assess whether the peptide inhibitor G7-18NATE-P altered cell migration into fibronectin, we used a modified Boyden chamber method *(7,22)*. The migration of Panc-1 pancreas cancer cells treated with G7-18NATE-P (5.7 cells, 95% CI = 2.3 to 9.0 cells) was statistically significantly less than that of cells treated with a control peptide (87.5 cells, 95% CI = 82.6 to 92.4 cells) ($P<.001$) or untreated Panc-1 pancreas cancer cells (Fig. 3, E). The Grb7 peptide inhibitor also reduced the migration of other human pancreatic cancer cell lines that overexpressed Grb7 peptide (such as MiaPaca2 and PK8 cells), but it did not reduce migration of other human pancreatic cancer cell lines that did not overexpress Grb7 (such as KLM1 cells) (Fig. 4; data not shown for PK8 cells). Thus, the peptide inhibitor G7-18NATE-P appeared to suppress Grb7 signaling via a pathway that is related to cell migration.

Effect of Grb7 Peptide Inhibitor on Metastasis of Pancreatic Cancer

To determine whether the Grb7 peptide inhibitor inhibited the metastasis of pancreatic cancer cells, we used a murine model of peritoneal metastasis *(26)*. We first injected Panc-1 human pancreatic cancer cells intraperitoneally into BALB/c *nu/nu* mice and then injected the Grb7 peptide inhibitor or a control peptide intraperitoneally every third day for a period of 2 weeks. Four weeks after the first injection of the Panc-1 cells, mice were killed, the numbers of peritoneal metastatic nodules were counted, and then each nodule was weighed. Fewer peritoneal metastases of the pancreas cancer cells were found in mice treated with the Grb7 peptide inhibitor than in mice treated with a control peptide (Fig. 5). Pancreatic cancer cells were found in the control mice but not in mice treated with the Grb7 peptide inhibitor (Fig. 5, A). In addition, the number of tumor nodules per mouse (control = 72.6 nodules, 95% CI = 55.8 to 89.4 nodules; Grb7 peptide = 3.2 nodules, 95% CI = 1.6 to 4.8 nodules; $P<.001$, *t* test) and the total nodule weight per mouse (control = 4.13 g, 95% CI = 3.40 to 4.86 g; Grb7 peptide = 0.19 g, 95% CI = 0.06 to 0.32 g; $P<.001$, *t* test) were statistically significantly lower in mice treated with the Grb7 peptide inhibitor than in mice treated with control peptide (Fig. 5, B). Similar results were found with other human pancreatic cancer cell lines that overexpressed Grb7 (such as MiaPaca2 cells) but not with lines that did not overexpress Grb7 (such as KLM1 cells) (data not shown). However, treatment with the Grb7 peptide inhibitor appeared to have no effect on the growth of subcutaneously injected pancreatic tumor (data not shown).

To investigate whether the Grb7 peptide inhibitor had adverse side effects, we injected BALB/c nu/nu mice with the Grb7 peptide inhibitor intraperitoneally every third day for 4 weeks and determined the body weight of the mice and the histologic changes of the major tissues, including liver, kidney, spleen, and lung. We found no clinically significant adverse effects, even when we injected a 10-fold higher concentration than was used to investigate metastasis.

Discussion

In this study, 61% of 36 pancreatic cancers were found to have higher levels of Grb7 protein than corresponding normal pancreatic tissue. The increased cellular levels of Grb7 appeared to be associated with regional lymph node metastatic spread of human pancreatic cancer ($P = .006$). Because the Grb7 SH2-mediated interactions might be an attractive candidate for the therapeutic targets of cancer invasion and metastasis *(17,22)*, we synthesized a thioether-cyclized peptide that selectively inhibited the interactions of Grb7 via its SH2 domain with protein tyrosine kinases *(20)*. In vitro, the Grb7 inhibitor blocked binding to FAK and phosphorylation of the endogenous Grb7 protein in human pancreatic cancer cells. In vivo in a mouse model of metastatic pancreatic cancer, the Grb7 peptide inhibitor completely attenuated cell migration (control = 81.8 cells migrated versus Grb7 peptide = 4.3 cells migrated; difference = 77.5 cells migrated, 95% CI = 64.2 to 90.7 cells migrated; $P<.001$) and peritoneal metastasis, as assessed by the number of tumor nodules (control = 72.6 nodules and Grb7 peptide = 3.2 nodules; difference = 69.4 nodules, 95% CI = 52.7 to 86.1 nodules; $P<.001$) or by the weight of the tumor nodules (control = 4.13 g and Grb7 peptide = 0.19 g; difference = 3.94 g, 95% CI = 3.34 to 4.54 g; $P<.001$). Our results suggest that the Grb7 peptide inhibitor might be a promising agent for molecular targeted therapeutics against the metastatic pancreatic cancer.

SH2 domains are relatively small protein modules of approximately 100 amino acids that recognize sequences containing

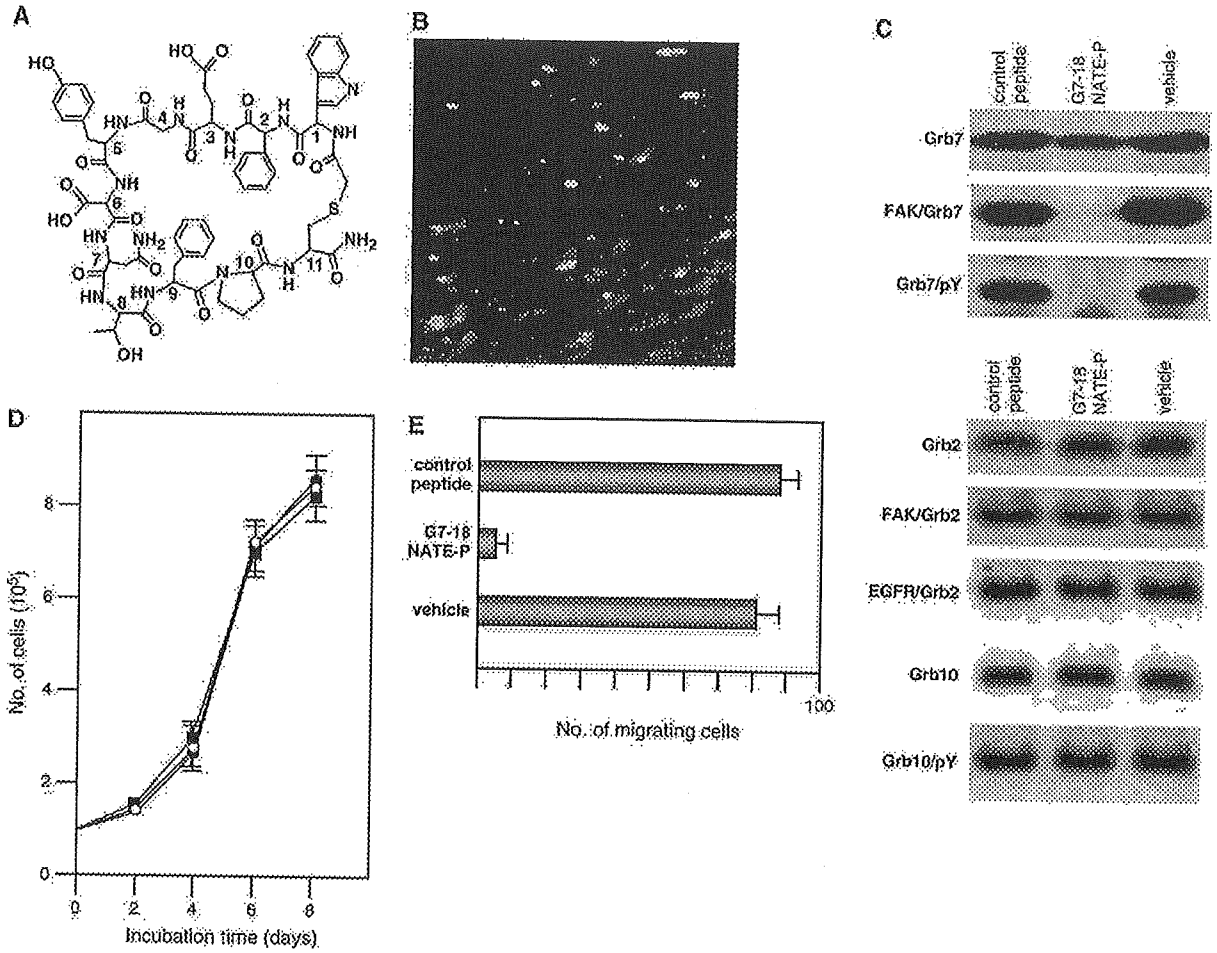

Fig. 3. Grb7 peptide inhibitor. **A)** Schematic structural formula of the modified nonphosphotyrosine cyclic Grb7 peptide inhibitor G7-18NATE (WFEGYDNTFPC). The cyclic peptide was synthesized by a thioether bond method, as described *(20)*. A modified form of G7-18NATE with a penetratin sequence attached (G7-18NATE-P; WFEGYDNTFPC-RQIKIWFQNRRMKWKK) was used for the in vivo studies. **B)** Intracellular localization of fluorescent-labeled G7-18NATE-P in the living cells of human pancreas cancer. After cells were incubated for 6 hours at 37 °C, the peptide (**green**) was detected by multichannel confocal laser–scanning microscopy in living Panc-1 cells. **C)** Immunoblot analysis. **Top)** Expression (blot Grb7), focal adhesion kinase (FAK) binding (blot FAK/Grb7), and tyrosyl phosphorylation of Grb7 protein (blot Grb7/pY). Panc-1 cells were plated on fibronectin (10 μg/mL) and then incubated with 10 mM control peptide (RQIKIWFQNRRMKWKK), 10 μM G7-18NATE-P, or vehicle for 1 hour at 37 °C. Grb7 was detected with anti-Grb7 protein antibody C-20. To detect the interaction between FAK and Grb7 protein (FAK/Grb7), 500 μg of cell lysate were immunoprecipitated with 10 μg of anti-FAK antibody for 6 hours at 4 °C, and the immunoprecipitate was subjected to sodium dodecyl sulfate–polyacrylamide gel electrophoresis, transferred onto Immobilon-P membranes (Millipore Corp.), and then immunoblotted with anti-Grb7 antibody. **Bottom)** Expression of Grb2 (blot Grb2), interaction of FAK with Grb2 (blot FAK/Grb2), interaction of epidermal growth factor receptor (EGFR) with Grb2 (blot EGFR/Grb2), expression of Grb10 (Grb10), and expression of tyrosyl-phosphorylated Grb10 (blot Grb10/pY). Grb2 was detected with anti-Grb2 monoclonal antibody. The interaction of FAK and Grb2 was detected by immunoprecipitation with anti-FAK antibody, followed by immunoblotting with anti-Grb2 antibody. The interaction of EGFR and Grb2 was detected by immunoprecipitation with anti-EGFR antibody, followed by immunoblotting with anti-Grb2 antibody. The expression of Grb10 was detected with anti-Grb10 polyclonal antibody. The expression of tyrosyl-phosphorylated Grb10 was detected by immunoprecipitation with anti-Grb10 antibody, followed by immunoblotting with anti-phosphotyrosine antibody. **D)** Growth curves. The proliferation of Panc-1 cells treated with control peptide, G7–18NATE-P, and vehicle was determined by counting the number of cells every other day for 8 days *(7,22)*. Data are expressed as averaged cell numbers, determined from three independent experiments with duplicate samples. **Error bars** = 95% confidence interval (CI). **E)** Fibronectin migration assay. We treated 1×10^4 Panc-1 cells with 10 μM G7-18NATE-P, 10 μM control peptide, or vehicle. The number of cells migrating into the fibronectin was determined for each culture, and the mean migration rate was determined from three experiments for duplicate samples. The mean number of cells migrating in cultures treated with G7-18NATE-P (5.7 cells, 95% CI = 2.3 to 9.0 cells) was statistically significantly less than that of cultures treated with a control peptide (87.5 cells, 95% CI = 82.6 to 92.4 cells) ($P<.001$). **Error bars** = 95% CIs. All statistical tests were two-sided.

phosphorylated tyrosine residues, thereby facilitating phosphorylation-dependent, protein–protein interactions that result in signal transduction *(4)*. Small-molecule inhibitors that can disrupt these interactions should be useful in modulating the function of the SH2-containing proteins and may ultimately be used as pharmaceutical agents *(5)*. The difficulty in designing cellularly active SH2 inhibitors has been the requirement of phosphotyrosine for high-affinity binding *(29)*. Peptide phage displays used to identify the ligands that bind to the SH2 domains have advantages over other methods, such as synthesis of phosphopeptides *(19)*. The peptide phage display method can be used to select phosphorylated ligands because bacteriophages lack tyrosine kinase activity, and thus the naturally occurring peptides on the phage contain no phosphorylated tyrosine residues *(30)*. The nonphosphorylated peptide that binds to the Grb7 SH2 domain has the advantage of in vivo stability over other SH2

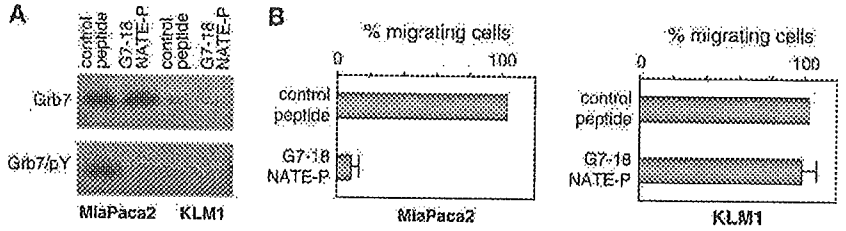

Fig. 4. Grb7 expression and effects of the Grb7 peptide inhibitor in human pancreatic cancer cells MiaPaca2 and KLM1. **A)** Overexpression and tyrosyl phosphorylation of Grb7 in fibronectin-stimulated pancreatic cancer cells MiaPaca2 and KLM1. Cells were treated with 10 μM control peptide or 10 μM G7-18NATE-P peptide inhibitor for 1 hour at 37 °C. Grb7 was detected by immunoblotting with anti-Grb7 polyclonal antibody. Phosphorylated Grb7 was detected by immunoprecipitation with anti-Grb7 antibody, followed by immunoblotting with anti-phosphotyrosine antibody. **B)** Cell migration assay in fibronectin. MiaPaca2 and KLM1 cells were treated with 10 μM G7-18NATE-P or 10 μM control peptide for 16 hours. The number of cells migrating into the fibronectin was determined by a modified Boyden chamber method. The mean migration rate, expressed as a percentage of migration with control peptide, was determined from three independent experiments with duplicate samples. **Error bars** = 95% confidence intervals (CIs) (MiaPaca2 = 7.7%, 95% CI = 3.1% to 12.4%; $P<.001$; KLM1 = 95.2%, 95% CI = 81.8% to 108.5%, $P = .395$). All statistical tests were two-sided.

ligands that possess a highly charged phosphate group *(20)*. When phosphate groups are attached to a macromolecule, the ability of the compound to enter cells is reduced, and the phosphorylated compound is instable in vivo because of the presence of endogenous phosphatases *(18)*. In vivo stability is important to the development of inhibitors that are cellularly active and clinically effective.

Recent advances in molecular biology have provided a detailed understanding of the molecular events in pancreatic carcinogenesis *(31,32)* and may now offer new approaches to the treatment of pancreatic cancer. As molecular targets are identified, novel agents that are specific for such targets can be designed that might improve the treatment of pancreatic cancer. Trials have evaluated several biological agents, including humanized monoclonal antibodies that inhibit members of the protein tyrosine kinase family, cetuximab that inhibits EGFR, and trastuzumab that inhibits erbB2 *(33,34)*. Other small molecules that inhibit the EGFR tyrosine kinase, such as ZD1839 and OSI-774, are also being investigated for activity in advanced pancreatic cancer *(35,36)*. Because Grb7 protein binds to many oncogenic protein tyrosine kinases, such as EGFR *(11)*, erbB2 *(10)*, erbB3 *(12)*, and erbB4 *(12)*, combination therapy with the protein tyrosine kinase-targeting agents and the Grb7 peptide inhibitor may be a novel therapeutic intervention.

Several limitations of this study must be noted. First, a small number of pancreatic cancer specimens was studied in our clinical investigation. Much larger clinical studies are required to determine whether Grb7 protein is associated with patient survival or outcome. Second, we could not determine the mechanism of action of the Grb7 peptide inhibitor in vivo. The actual effects of the peptide on actively invading tumors should be analyzed. Finally, the actual cellular and molecular functions of Grb7 have not been defined in detail *(16,17)*. Guan and colleagues *(37)* have reported that the association of Grb7 with phosphatidylinositol 3-kinase mediates the signal transduction pathways in FAK-induced cell migration. Recently, PREL1, another homologue of Grb7 and Mig-10 proteins, was found to bind to the actin cytoskelton via Ena/vasodilator-stimulated phosphoproteins, which are important regulators of the actin polymerization machinery *(38)*. Further analyses are required to identify the downstream targets of the Grb7-meidated signaling pathways to cancer metastasis.

In view of the evidence presented on the relationship between Grb7 expression and tumor progression, potent Grb7 antagonists may be promising anticancer agents for treatment of human cancers *(16)*. Because of the antimetastatic activity and the low toxicity of the Grb7 peptide inhibitor in mice, the potential of this inhibitor or its analogues should be investigated in additional preclinical experiments as treatments for human cancers that

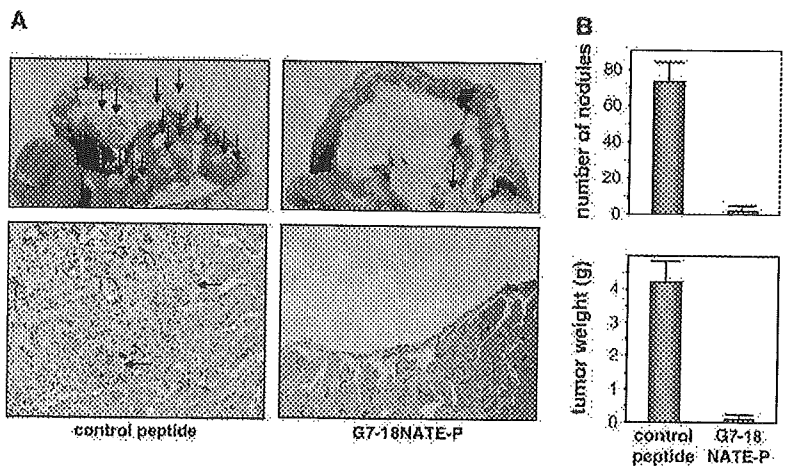

Fig. 5. Grb7 peptide inhibitor and metastasis. BALB/c *nu/nu* mice were inoculated intraperitoneally with Panc-1 human pancreatic cancer cells *(22)*. **A)** Representative peritoneal metastases of Panc-1 cells in mice treated with the control peptide **(left)** or with the Grb7 peptide inhibitor G7-18NATE-P **(right)**. **Upper)** Peritoneal metastases. **Arrows** = nodules. **Lower)** Representative sections of Panc-1 tumor cells invading the parietal peritoneum in mice treated with the control peptide **(arrows, left)** but not in mice treated with G7-18NATE-P **(right)**. Similar effects were detected with other human pancreas cancer cell lines examined. **B)** Number of nodules and total weight of metastatic nodules per mouse. **Upper)** Number of nodules. The number of nodules was statistically significantly lower in mice treated with the Grb7 inhibitor (3.2 nodules, 95% confidence interval [CI] = 1.6 to 4.8 nodules; $P<.001$, *t* test) than in mice treated with control peptide (control = 72.6 nodules, 95% CI = 55.8 to 89.4 nodules) ($P<.001$, *t* test). **Lower)** Total weight of nodules. The total weight of nodules was statistically significantly lower in mice treated with the Grb7 peptide inhibitor (Grb7 peptide = 0.19 g, 95% CI = 0.06 to 0.32 g) than in mice treated with control peptide (control = 4.13 g, 95% CI = 3.40 to 4.86 g) ($P<.001$, *t* test). **Error bars** = 95% CIs. All statistical tests were two-sided.

overexpress Grb7 *(17)*. The Grb7 peptide inhibitor should also be evaluated as a lead compound for the development of new drugs to treat diseases in which Grb7 is overexpressed, and it may also aid in elucidating the function of Grb7 in cancer cells *(18)*. In addition, clinical studies should be designed to evaluate the effects of the peptide inhibitor in humans against pancreatic cancer and other cancers that overexpress Grb7, such as esophageal *(6)*, gastric *(9)*, and breast *(10)* cancers.

References

(1) Li D, Xie K, Wolff R, Abbruzzese JL. Pancreatic cancer. Lancet 2004; 363:1049–57.

(2) Bardeesy N, DePinho RA. Pancreatic cancer biology and genetics. Nat Rev Cancer 2002;2:897–909.

(3) Blume-Jensen P, Hunter T. Oncogenic kinase signalling. Nature 2001; 411:355–65.

(4) Pawson T. Specificity in signal transduction: from phosphotyrosine-SH2 domain interactions to complex cellular systems. Cell 2004;116:191–203.

(5) Machida K, Mayer BJ. The SH2 domain: versatile signaling module and pharmaceutical target. Biochim Biophys Acta 2005;1747:1–25.

(6) Tanaka S, Mori M, Akiyoshi T, Tanaka Y, Mafune K, Wands JR, et al. Coexpression of Grb7 with epidermal growth factor receptor or Her2/erbB2 in human advanced esophageal carcinoma. Cancer Res 1997;57:28–31.

(7) Tanaka S, Mori M, Akiyoshi T, Tanaka Y, Mafune K, Wands JR, et al. A novel variant of human Grb7 is associated with invasive esophageal carcinoma. J Clin Invest 1998;102:821–7.

(8) Manser J, Roonprapunt C, Margolis B. C. elegans cell migration gene mig-10 shares similarities with a family of SH2 domain proteins and acts cell nonautonomously in excretory canal development. Dev Biol 1997;184: 150–64.

(9) Akiyama N, Sasaki H, Ishizuka T, Kishi T, Sakamoto H, Onda M, et al. Isolation of a candidate gene, CAB1, for cholesterol transport to mitochondria from the c-ERBB-2 amplicon by a modified cDNA selection method. Cancer Res 1997;57:3548–53.

(10) Stein D, Wu J, Fuqua SAW, Roonprapunt C, Yajnik V, Moskow JJ, et al. The SH2 domain protein GRB-7 is co-amplified, overexpressed and in a tight complex with HER2 in breast cancer. EMBO J 1994;13:1331–40.

(11) Margolis B, Silvennoinen O, Comoglio F, Roonprapunt C, Skolnik E, Ullrich A, Schlessinger J. High-efficiency expression/cloning of epidermal growth factor-receptor-binding proteins with Src homology 2 domains. Proc Natl Acad Sci USA 1992;89:8894–8.

(12) Fiddes RJ, Campbell DH, Janes PW, Sivertsen SP, Sasaki H, Wallasch C, Daly RJ. Analysis of Grb7 recruitment by heregulin-activated erbB receptors reveals a novel target selectivity for erbB3. J Biol Chem 1998;273: 7717–24.

(13) Han DC, Shen TL, Guan JL. Role of Grb7 targeting to focal contacts and its phosphorylation by focal adhesion kinase in regulation of cell migration. J Biol Chem 2000;275:28911–7.

(14) Feldner JC, Brandt BH. Cancer cell motility—on the road from c-erbB-2 receptor steered signaling to actin reorganization. Exp Cell Res 2002;272: 93–108.

(15) McLean GW, Carragher NO, Avizienyte E, Evans J, Brunton VG, Frame MC. The role of focal-adhesion kinase in cancer—a new therapeutic opportunity. Nat Rev Cancer 2005;5:505–15.

(16) Daly RJ. The Grb7 family of signalling proteins. Cell Signal 1998;10: 613–8.

(17) Han DC, Shen TL, Guan JL. The Grb7 family proteins: structure, interactions with other signaling molecules and potential cellular functions. Oncogene 2001;20:6315–21.

(18) Pero SC, Daly RJ, Krag DN. Grb7-based molecular therapeutics in cancer. Expert Rev Mol Med 2003;5:1–11.

(19) Oligino L, Lung FD, Sastry L, Bigelow J, Cao T, Curran M, et al. Nonphosphorylated peptide ligands for the Grb2 Src homology 2 domain. J Biol Chem 1997;272:29046–52.

(20) Pero SC, Oligino L, Daly RJ, Soden AL, Liu C, Roller PP, et al. Identification of novel non-phosphorylated ligands, which bind selectively to the SH2 domain of Grb7. J Biol Chem 2002;277:11918–26.

(21) Joliot A, Pernelle C, Deagostini-Bazin H, Prochiantz A. Antennapedia homeobox peptide regulates neural morphogenesis. Proc Natl Acad Sci USA 1991;88:1864–8.

(22) Tanaka S, Sugimachi K, Kawaguchi H, Saeki H, Ohno S, Wands JR, et al. Grb7 signal transduction protein mediates metastatic progression of esophageal carcinoma. J Cell Physiol 2000;183:411–5.

(23) Walch A, Specht K, Braselmann H, Stein H, Siewert JR, Hopt U, et al. Coamplification and coexpression of GRB7 and ERBB2 is found in high grade intraepithelial neoplasia and in invasive Barrett's carcinoma. Int J Cancer 2004;112:747–53.

(24) Scherer LJ, Ross JJ. Approaches for the sequence-specific knockdown of mRNA. Nat Biotechnol 2003;21:1457–60.

(25) Bodanszky M, Bodanszky A, editors. The practice of peptide synthesis. 2nd rev. ed. New York (NY): Springer-Verlag; 1994.

(26) Tanaka S, Mori M, Sakamoto Y, Makuuchi M, Sugimachi K, Wands JR. Biologic significance of angiopoietin-2 expression in human hepatocellular carcinoma. J Clin Invest 1999;103:341–5.

(27) Tanaka S, Wands JR. A carboxy-terminal truncated IRS-1 dominant negative protein reverses the human hepatocellular carcinoma malignant phenotype. J Clin Invest 1996;98:2100–8.

(28) Safran H, Steinhoff M, Mangray S, Rathore R, King TC, Chai L, et al. Overexpression of the HER-2/neu oncogene in pancreatic adenocarcinoma. Am J Clin Oncol 2001;24:496–9.

(29) Shakespeare WC. SH2 domain inhibition: a problem solved? Curr Opin Chem Biol 2001;5:409–15.

(30) Beeler JF, LaRochelle WJ, Chedid M, Tronick SR, Aaronson SA. Prokaryotic expression cloning of a novel human tyrosine kinase. Mol Cell Biol 1994;14:982–8.

(31) Thayer SP, di Magliano MP, Heiser PW, Nielsen CM, Roberts DJ, Lauwers GY, et al. Hedgehog is an early and late mediator of pancreatic cancer tumorigenesis. Nature 2003;425:851–6.

(32) Stanger BZ, Stiles B, Lauwers GY, Bardeesy N, Mendoza M, Wang Y, et al. Pten constrains centroacinar cell expansion and malignant transformation in the pancreas. Cancer Cell 2005;8:185–95.

(33) Xiong HQ, Rosenberg A, LoBuglio A, Schmidt W, Wolff RA, Deutsch J, et al. Etuximab, a monoclonal antibody targeting the epidermal growth factor receptor, in combination with gemcitabine for advanced pancreatic cancer: a multicenter phase II trial. J Clin Oncol 2004;22:2610–6.

(34) Safran H, Iannitti D, Ramanathan R, Schwartz JD, Steinhoff M, Nauman C, et al. Herceptin and gemcitabine for metastatic pancreatic cancers that overexpress HER-2/neu. Cancer Invest 2004;22:706–12.

(35) Fjallskog ML, Lejonklou MH, Oberg KE, Eriksson BK, Janson ET. Expression of molecular targets for tyrosine kinase receptor antagonists in malignant endocrine pancreatic tumors. Clin Cancer Res 2003;9:1469–73.

(36) Iannitti D, Dipetrillo T, Akerman P, Barnett JM, Maia-Acuna C, Cruff D, et al. Erlotinib and chemoradiation followed by maintenance erlotinib for locally advanced pancreatic cancer: a phase I study. Am J Clin Oncol 2005;28:570–5.

(37) Shen TL, Han CH, Guan JL. Association of Grb7 with phosphoinositides and its role in the regulation of cell migration. J Biol Chem 2002;277: 29069–77.

(38) Jenzora A, Behrendt B, Small JV, Wehland J, Stradal TE. PREL1 provides a link from Ras signalling to the actin cytoskeleton via Ena/VASP proteins. FEBS Lett 2005;579:455–63.

Notes

This work was supported by a grant-in-aid from the Ministry of Education, Science, Sports and Culture of Japan, Japan Science and Technology Agency and by grant R01 CA80790 from the National Institutes of Health. S. Tanaka is a recipient of the Japan Cancer Society Incitement Award and the ISCRT Award for Cancer Research.

Manuscript received October 24, 2005; revised January 17, 2006; accepted February 17, 2006.

Frag1, a homolog of alternative replication factor C subunits, links replication stress surveillance with apoptosis

Hideshi Ishii*, Taeko Inageta*, Koshi Mimori†, Toshiyuki Saito‡, Hiroki Sasaki§, Masaharu Isobe¶, Masaki Mori†, Carlo M. Croce||**, Kay Huebner||, Keiya Ozawa*, and Yusuke Furukawa*

*Center for Molecular Medicine, Jichi Medical School, Tochigi 329-0498, Japan; †Institute of Bioregulation, Kyushu University, Ohita 874-0838, Japan; ‡Transcriptome Profiling Group, National Institute for Radiological Science, Chiba 263-8555, Japan; §Genetics Division, National Cancer Center Research Institute, Tokyo 104-0045, Japan; ¶Faculty of Engineering, Toyama University, Toyama 930-8555, Japan; and ||Department of Molecular Virology, Immunology, and Medical Genetics, Comprehensive Cancer Center, Ohio State University, Columbus, OH 43210

Contributed by Carlo M. Croce, May 23, 2005

We report the identification and characterization of a potent regulator of genomic integrity, mouse and human *FRAG1* gene, a conserved homolog of replication factor C large subunit that is homologous to the alternative replication factor C subunits Elg1, Ctf18/Chl12, and Rad24 of budding yeast. *FRAG1* was identified in a search for key caretaker genes involved in the regulation of genomic stability under conditions of replicative stress. In response to stress, Atr participates in the down-regulation of *FRAG1* expression, leading to the induction of apoptosis through the release of Rad9 from damaged chromatin during the S phase of the cell cycle, allowing Rad9–Bcl2 association and induction of proapoptotic Bax protein. We propose that the Frag1 signal pathway, by linking replication stress surveillance with apoptosis induction, plays a central role in determining whether DNA damage is compatible with cell survival or whether it requires cell elimination by apoptosis.

genomic integrity | Bcl2 | Rad9 | Atr | Rb

Replicative stress causes replication fork stalling or arrest, which can occur in yeast at naturally occurring sequences, such as replication fork barriers and replication slow zones (1). When damage is severe or the natural order of DNA replication is perturbed, DNA double-strand breaks can occur (2). Such events can trigger cellular checkpoints, allowing time for repair of damage before cell cycle progression (2). When the breaks are fixed or the damage is compatible with cell survival, double-strand breaks can give rise to the fixed chromosomal aberrations observed in cancer cells, such as translocations, inversions, amplifications, and deletions. Accumulated aberrations of caretaker pathways in concert with alterations of gatekeeper tumor suppressors give rise to transformed cells that acquire selective growth and survival advantages (3). Thus, the pathology of stalled or collapsed replication forks is important for understanding the role of faithful regulation of replication in preventing carcinogenesis.

Genotoxic stress-induced replication stalling activates checkpoint-signaling pathways that block cell cycle progression, control DNA repair, or trigger apoptosis (4) through membrane death receptors and the endogenous mitochondrial death pathways (5). Rad9 protein is involved in the control of the DNA damage-induced checkpoint (6). Studies in yeast and human cells have shown that Rad9 interacts with Hus1 and Rad1 in the 9-1-1 complex, which is a heterotrimeric complex and acts as a proliferating cell nuclear antigen-like sliding clamp (4, 7). In response to DNA damage, the 9-1-1 complex is loaded around DNA lesions by Rad17, which binds to chromatin before damage (8) and facilitates Atr-mediated phosphorylation and activation of Chk1 kinase to arrest cell cycle. Rad9 can participate in signaling apoptosis by interacting with antiapoptotic Bcl-2 family proteins Bcl-2 and Bcl-X_L but not with proapoptotic Bax and Bad (9). The interaction of Bcl2 with Bax prevents Bax from inducing cytochrome *c* release and cell death, and the Bax/Bcl2 ratio is crucial for regulation of apoptosis (10). Because the 9-1-1 clamp is also involved in DNA repair (7), the Rad9 complex is thought to play a key role in coordinating multiple functions of checkpoint activation, DNA repair, and apoptosis.

In this study, we report the identification and characterization of the *FRAG1* gene, which encodes a 1,820-aa mouse and 1,844-aa human conserved, uncharacterized protein homolog of the large replication factor C (RFC) subunit Rfc1 (861 aa) and the alternative RFC subunits Elg1 (791 aa), Ctf18/Chl12 (741 aa), and Rad24 (659 aa; Rad17 in human) in budding yeast. Elg1 (enhanced levels of genome instability), a RFC homolog, which forms an alternative RFC complex with Rfc2–Rfc5, was discovered through budding yeast genome-wide synthetic genetic interaction screening of mutants of replication fork-progression genes (11) and through the study of mutants exhibiting high levels of Ty recombination (12, 13). The Elg1 complex is distinct from RFCs for DNA replication, the DNA damage checkpoint, and sister chromatid cohesion (11–14). We have now isolated the mammalian *FRAG1* gene, characterized the function of Frag1 protein in higher eukaryotes, compared it with homologous DNA replication and damage response proteins of simpler organisms, and shown that it is involved in a Rad9-related damage checkpoint, a pathway that is important in determining whether DNA damage will be tolerated or whether the damaged cells will be eliminated by apoptosis.

Materials and Methods

Cell Culture. For synchronization by double thymidine block, after culture in medium with 10% FCS/DMEM containing 2.5 mM thymidine for 24 h (the first block), cells were washed with PBS, grown for 10 h in fresh DMEM/10% FCS, cultured 16 h in 2.5 mM thymidine (the second block) and then incubated as indicated without thymidine. Flow cytometric analysis after BrdUrd incorporation showed that >90% cells entered S phase 2–8 h after release. Cell viability was assessed by visualization of cell morphology, trypan blue, or erythrosine B exclusion, Hoescht 33342 vital staining, and flow-assisted cytometric analysis.

Genotoxic Stress and Colony Assay. For synchronized cells, 0.4 μM aphidicolin (Sigma) in 0.2% DMSO was included in the thymidine medium for 16 h of the second synchronization. Medium was exchanged for thymidine-free medium containing 2.2 μM caffeine (Sigma) and 0.4 μM aphidicolin for an indicated period. For DNA

Abbreviations: MEF, mouse embryonic fibroblast; MMS, methyl methanesulfonate; RFC, replication factor C; siRNA, short interfering RNA.

Data deposition: The sequences reported in this paper have been deposited in the GenBank database (accession nos. AY557610 and AY557611).

**To whom correspondence should be addressed at: Comprehensive Cancer Center, Ohio State University, Wiseman Hall, Room 385L, 410 West 12th Avenue, Columbus, OH 43210. E-mail: carlo.croce@osumc.edu.

damage, the DNA alkylating agent methyl methanesulfonate (MMS) (15) was added in the medium at indicated conditions. For UV irradiation, 60–70% confluent monolayer cells were irradiated with UV-C emitted by germicidal lamps (GL-15, NIPPO Electronic, Tokyo, Japan) emitting at predominantly 254 nm. For colony assay, cells were cultured in medium with MMS for 1 h, washed, and plated in DMEM/10% FBS with 1.5% methylcellulose; colonies were counted 10 days later. For radiation, cells were exposed to ^{137}Cs [661 keV (1 eV = 1.602×10^{-19} J) at indicated doses] and assessed as indicated.

Plasmids and Small Interfering RNAs (siRNAs). pcDNA4V5 DNA (Clontech), was ligated in-frame with F1 (nucleotide positions from the first coding methionine, 1–1440), F2 (1400–1839), F3 (1794–3177), F4 (2697–3975), or FZ (3972–5535) DNA fragments of human Frag1 cDNA. Wild-type pBJF-FLAG-ATR (pBJF-FLAG-ATRwt), kinase-dead pBJF-FLAG-ATR (pBJF-FLAG-ATRkd) [from S. Schreiber (Harvard University, Cambridge, MA) and K. Cimprich (Stanford University, Stanford, CA)], HA-Rad9, Flag–N-terminally deleted Rad9 [Rad9-δN; from H-G. Wang (University of South Florida, Tampa)], and pCAGGS-hbcl-2 [from Y. Eguchi and Y. Tsujimoto (Osaka University, Osaka, Japan)] were used for transfection. GST-fusion (Amersham Pharmacia) was used for protein expression.

Construction of siRNA-expression plasmids was based on the U6 siRNA expression vector (Takara, Mie, Japan), which includes a mouse U6 promoter, a puromycin-resistance gene, and two BspMI sites. Two sets of the sense and antisense oligonucleotides (Table 1, which is published as supporting information on the PNAS web site) were annealed and ligated into the vector. U6 siRNA-Frag1 plasmids were transfected into cells by using TransIT-TKO transfection reagent (Mirus, Madison, WI) and selected in 1 μg/ml puromycin. Colonies were picked, and expression was evaluated by RT-PCR and immunoblot analysis. siRNA expression vectors with EGFP antisense or without inserts were used as controls (Takara). Oligo siRNAs for mouse p73, Atr, and luciferase were used as recommended (Santa Cruz Biotechnology).

cDNA Isolation and RNA Analysis. RNAs were extracted with a Qiagen (Valencia, CA) kit and cDNAs synthesized from 2 μg of poly(A)$^+$ RNA with Superscript II reverse transcriptase and oligo(dT) and random primers (Invitrogen). Differentially expressed genes were isolated with a cDNA subtraction kit (Clontech). After two rounds of hybridizations, cDNAs were amplified, ligated to vector, and sequenced.

For hybridization, 5-μg RNAs were fractionated by agarose gel electrophoresis, transferred to Nylon membrane, and hybridized with the following probes: cDNAs of the peptide coding region of *FRAG1* (N- and C-terminal), *RFC1*, *CTF18*, *DCC*, and *RAD17*, which were amplified by RT-PCR, subcloned, and sequenced. Filters were washed and exposed to x-ray film.

Protein Analysis and Fractionation. For immunoprecipitation, cells were harvested and 500-μg samples of cell lysates, after being precleared with protein G-Sepharose beads, were incubated with 3–4 μg of specific antibody overnight. Antigen–antibody complex was immobilized on protein G-Sepharose beads, and the beads were washed five times in lysis buffer. Bound proteins were eluted by boiling and subjected to SDS/PAGE and immunoblotting. Immunofluorescence staining and confocal analysis were performed by culturing cells in chambered slides, followed by methanol fixation, 0.05% Triton X-100 treatment, and staining with first and secondary antibodies. Primary antibodies used were anti-human p53 (BD Biosciences), phosphorylated p53 (Ser-15) (BD Biosciences), Mdm2 (Santa Cruz Biotechnology), Rb (BD Biosciences), Rad9 (Santa Cruz Biotechnology), phospho-H2AX (catalog no. 07-164; Upstate Biotechnology, Chicago), mitochondria (Chemicon), Bax (catalog no. 2772, Cell Signaling Technology; N-20, Santa Cruz Biotechnology), Atr (ab-2, EMD Biosciences, San Diego; catalog no. sc-1887, Santa Cruz Biotechnology), Orc2 (BD Biosciences), cytochrome *c* (Pharmingen), phospho-H2AX (catalog no. 05-636; Upstate Biotechnology), Grb2 (BD Biosciences), V5 (Invitrogen), Flag (Sigma), and actin (ICN, Irvine CA), which were detected with secondary antisera in an enhanced chemiluminescence system (ECL, Amersham Biosciences). Rabbit polyclonal anti-Frag1 antiserum was developed against peptide sequences mouse 345 CSLSDPENEQPVQKRKSN 362 and affinity-purified. *In vitro* transcription/translation was performed with a rabbit reticulocyte system (Amersham Biosciences) by labeling cDNAs cloned by RT-PCR amplification with [^{35}S]methionine (Amersham Biosciences). Proteins were incubated in 100 μl of binding buffer containing 150 mM NaCl, 0.1% Tween 20, 0.75 mg/ml BSA, 50 mM Tris·HCl (pH 8.0), 5 mM EDTA, and 10% (vol/vol) glycerol. For pulling down, glutathione–agarose bead-bound proteins were subjected to SDS/PAGE after being washed five times, and the gels were exposed to x-ray film. Cellular fractions were prepared as described in ref. 16.

Results and Discussion

Identification of FRAG1, a Gene Differentially Expressed After Replication Stress. DNA replication guarantees the duplication of the genome and requires concerted, dynamic changes of expression of specific gene products, which regulate the integrity of replication and surveillance of the genome for damage (17). When replication forks encounter damage in the DNA strands, stalling or arrest can result, leading to stimulation of the downstream checkpoint to initiate cell cycle arrest or apoptosis (1); however, the molecular mechanisms that sense stalled replication are not understood fully. To study differentially expressed genes in conditions of replication stress, synchronized mouse embryonic fibroblasts (MEFs) were exposed to aphidicolin, a DNA polymerase inhibitor, and harvested 4 h (in mid-S phase) after release from a double thymidine block. RNA was extracted from MEFs, and subtractive cDNA hybridization was performed to identify genes differentially expressed in the presence or absence of aphidicolin (Fig. 7*A*, which is published as supporting information on the PNAS web site). BLAST database searches indicated that 155 clones that we isolated and sequenced included 86 clones (55%) identical to mouse ESTs (>95% homologous over 200 bp). The 86 clones included redundant clones; 13 clones corresponded to an overlapped cDNA contig (denoted as FRAG1/N), seven clones corresponded to a contig (FRAG1/C), and five clones corresponded to *RFC1* cDNA. Interestingly, database searches indicated that FRAG1/N and FRAG1/C are located adjacent to each other (C130052G03Rik, GenBank accession no. XM_282980; Gm17, GenBank accession no. XM_111221) on mouse chromosome 11. Database searches for human orthologs of the mouse clones showed that the orthologs are parts of a continuous gene, FLJ12735 (GenBank accession no. NM_024857), at human chromosome 17q11.2. RT-PCR amplification indicated that those "two" mouse transcripts span a gene, suggesting that the two transcripts, FRAG1/N and FRAG1/C came from one gene, *FRAG1* (Ctf18/Rad24/Elg1-related gene 1). We have focused on characterization of the *FRAG1* gene.

Alteration of FRAG1 Expression. Northern blot analysis was performed with replication-related genes *RFC1*, *RAD17*, and *CTF18*, as well as FRAG1/N and FRAG1/C as probes. Synchronized MEFs were treated with aphidicolin or MMS (a DNA alkylating agent), agents that cause stalled DNA replication (15). Expression of FRAG1/N and FRAG1/C was markedly down-regulated by aphidicolin or MMS treatment, whereas the effect on *RFC1*, *Rad17*, and *CTF18* genes was less apparent after MMS treatment (Fig. 1*A*). RNA blot with cDNA probes of N- and C-terminal portions of *FRAG1* (FRAG1/N and FRAG1/C) (Fig. 1*C*) detected a predominant transcript of ≈9 kb expressed ubiquitously in 12 murine cell lines (Fig. 1*B*). To assess the stability of the *FRAG1* transcript,

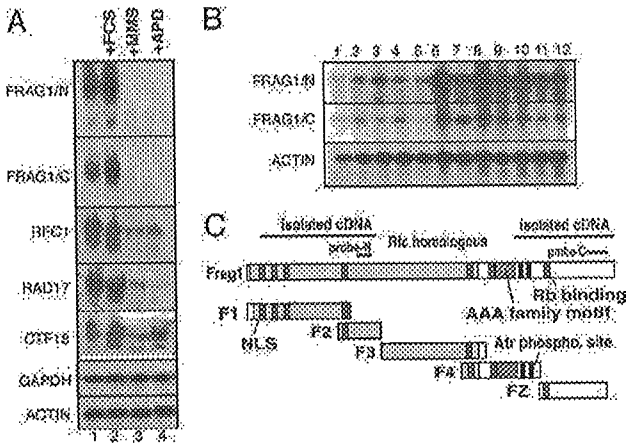

Fig. 1. Expression of the *FRAG1* gene. (*A*) RNA blot analysis. Synchronized MEFs were treated with aphidicolin, and 20 μg of each of the total RNAs were loaded on the gel, transferred to membrane, and hybridized to probes as indicated. (*B*) Frag1 expression in various mouse cell lines. Shown are poly(A)$^+$ RNA from the following sources: lane 1, PU5–1.8 (lymphoid tumor); lane 2, RAW264.7 (leukemia-virus induced tumor); lane 3, K-BALB (Kirsten murine leukemia virus-transformed fibroblast); lane 4, 3T3 (fibroblast); lane 5, L-M (murine L cells, transformed adipose connective tissue); lane 6, P19 (teratocarcinoma); lane 7, Hepa 1-6 (hepatoma); lane 8, R1.1 (T cell lymphoma); lane 9, L1210 (lymphocytic leukemia); lane 10, P388D1 (lymphoma); lane 11, P815 (mastcytoma); and lane 12, NB41A3 (neuroblastoma). (*C*) A map of Frag1 fragments. F1, F2, F3, F4, and FZ are cDNA fragments used in the study. Location of probes Frag1/N and Frag1/C in the cDNA are indicated. Rb binding motif LxCxE and two putative Atr-phosphorylation sites are located near a region homologous to the AAA family. Two locations of cDNA fragments, which were isolated through subtractive hybridization (nucleotide positions from the first methionine, 321–1835 and 3750–5388) are shown, and two probes for RNA blot analysis, which were synthesized by PCR amplification (nucleotide positions from the first methionine, 1580–1830 and 5130–5380) are shown. NLS, nuclear localization motifs.

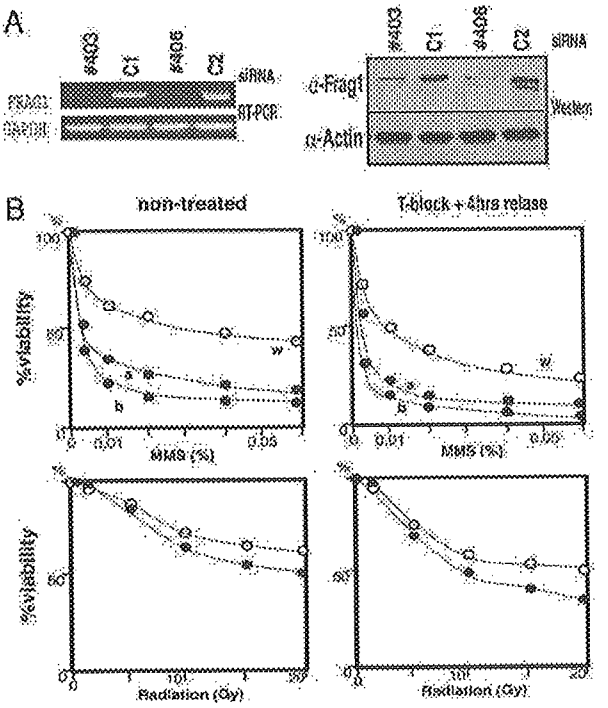

Fig. 2. Down-regulation of Frag1 expression sensitizes cells to replicative stress. (*A*) Down-regulation of *FRAG1* by siRNA. MEFs were transfected by U6 siRNA expression vector against FRAG1 and grown in selective medium. RNAs and protein lysates were extracted and analyzed by RT-PCR and immunoblot. Results of two independent experiments of *FRAG1* siRNA clones (#403 and #406) are shown. C, mock control siRNA. (*B*) Colony survival assay after exposure to MMS. Synchronized (*Right*) or asynchronized (*Left*) cells (1×10^6) were cultured in thymidine-free medium for 2 h to allow S-phase entrance. (*Upper*) MMS was added at the indicated concentrations for an additional 1 h, and cells were washed. (*Lower*) For radiation, cells were exposed at the indicated doses. Cells were plated in DMEM containing 1.5% methylcellulose, and colonies were counted 10 days after treatment. The percentage of survival was determined relative to the numbers of colonies from untreated cells. Lines labeled a and b indicate experiments with two independent siRNAs; lines labeled w indicate mock.

cells treated with actinomycin D to inhibit *de novo* RNA synthesis in medium with or without aphidicolin were harvested at serial time points and assessed for *FRAG1/N*, *FRAG1/C*, *CTF18*, *RFC*, and *RAD17* mRNA, indicating that the half-life of *FRAG1* mRNA appears to be <4 h after exposure to aphidicolin. In contrast, the half-life of *CTF18*, *RFC*, and *RAD17* mRNAs was >15 h, suggesting that *FRAG1* mRNA appeared less stable than transcripts of the other replication-related genes examined (Fig. 7 *B–E*).

Database searches indicated that the putative Frag1 protein has a conserved region homologous to a large subunit of RFC, which is considered an ortholog of the alternative RFC subunits, Elg1, Ctf18/Chl12, and Rad24 (Rad17 in fission yeast and human) of budding yeast (Fig. 1*C*) (11–14). Frag1 has a conserved AAA family motif, a hallmark of the ATPase family associated with various cellular activities, including chaperone-like functions that assist in the assembly, operation, or disassembly of protein complexes. Comparison of the mouse and human Frag1 amino acid sequences indicated that they conserve putative Atr-phosphorylation sites (mouse Frag1 at Ser-1150 and Ser-1168 and human Frag1 at Ser-1169 and Ser-1187) (18, 19), and a putative Rb binding site with a Leu-x-Cys-x-Glu (LxCxE) motif (amino acids 1409–1413 of mouse and 1428–1432 of human) (20).

Reduction of Frag1 Protein Increases Sensitivity to DNA Damage. Studies of budding yeast have shown that elg1Δ mutants are sensitive to DNA damage, suggesting that Elg1-RFC functions in the DNA damage response (11, 12). To study the effect of reduced expression of mammalian Frag1 protein, we performed siRNA experiments to inhibit expression of endogenous Frag1. RT-PCR and immunoblot study showed that cells transfected with the siRNA vector and selected in puromycin medium showed a marked reduction of Frag1 gene product (Fig. 2*A*). *FRAG1* siRNA transfectants were exposed to MMS or to γ-irradiation, and colony survival was assayed. Compared with control siRNA transfectants, two independent *FRAG1* siRNA transfectants showed enhanced sensitivity to replication stress, which was apparent in synchronized MEFs, suggesting that the damage activated the S phase checkpoint (Fig. 2*B*). The difference between siRNA knock-down and control cells after MMS treatment is more pronounced than differences observed after γ-irradiation. It is suggested that reduction of Frag1 increased the sensitivity to MMS.

Frag1 siRNA Inhibition Leads to Activation of Caspase and BAX. Immuunoblot analysis of Frag1 protein expression showed that Frag1 was reduced 2–6 h after exposure to aphidicolin or MMS, a reduction more rapid than for actin or Rad17 in MMS (Fig. 3*A*). Because involvement of Frag1 in cellular responses to DNA damage is suggested, we assessed the activation of proapoptotic proteins. Immunoblot analysis showed caspase 7 activation in *FRAG1* siRNA transfectants but not in control siRNA transfectants (Fig. 8*A*, which is published as supporting information on the PNAS web site). Bax protein expression with slow mobility was induced in two independent *FRAG1* siRNA transfectants 8 h after release from double thymidine cell cycle block and was markedly induced in

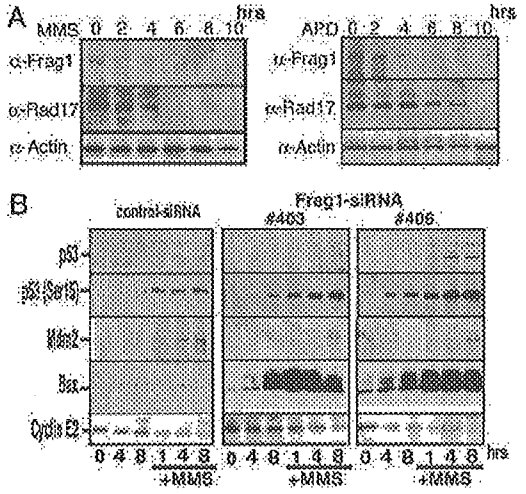

Fig. 3. Frag1 is involved in genotoxic response. (*A*) Frag1 down-regulation by genotoxic stress. MEFs were cultured in medium with 0.4 nM aphidicolin or 0.01% MMS for the indicated times. Cells were harvested, and lysates were subjected to SDS/PAGE and immunoblot analysis with antisera as indicated. (*B*) Frag1 knock-down sensitizes cells to genotoxic stress. Two independent Frag1 siRNA MEF clones (#403 and #406) synchronized in G_1 and grown in thymidine-free medium with or without exposure to MMS were harvested at the indicated times after release in thymidine-free medium. Protein lysates were immunoblotted with antibodies as indicated. Mismatched siRNA served as control.

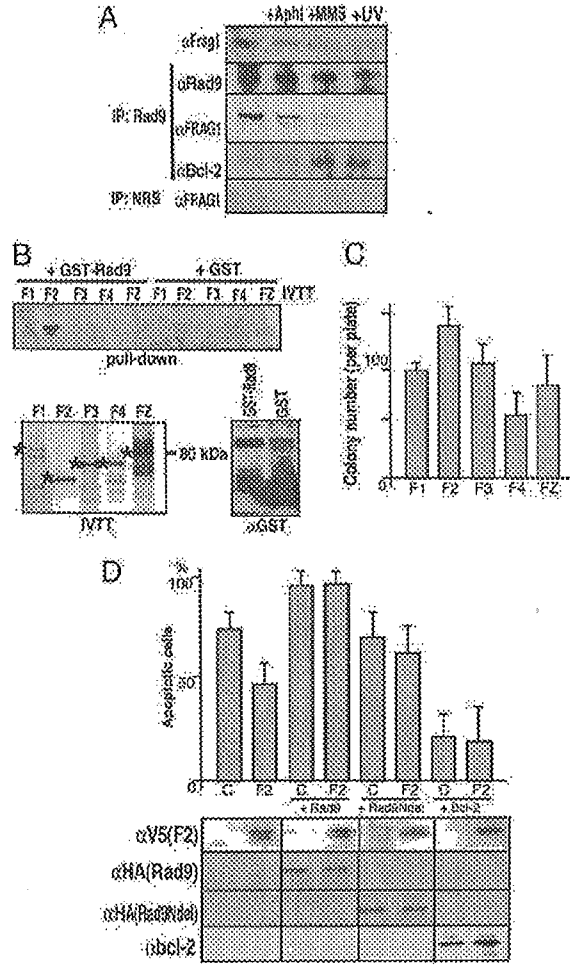

Fig. 4. Frag1 is involved in the Rad9–Bcl2 pathway. (*A*) Coimmunoprecipitation of Frag1, Rad9, and Bcl2. MEFs were grown in medium with 0.4 μM aphidicolin (Aphi) or 0.01% MMS for 24 h or exposed to 8 J/m^2 UV radiation and cultured for 24 h before harvesting. The leftmost lane is without treatment. Protein lysates were extracted and immunoprecipitated (IP) with anti-Rad9 or normal rabbit serum (NRS), followed by immunoblot with Frag1, Rad9, or Bcl2 antisera. (*B*) Pull down of *in vitro* transcribed and translated (IVTT) F1, F2, F3, F4, and FZ fragments of Frag1 by GST–Rad9 fusion protein. *In vitro* transcribed and translated products were labeled with [^{35}S]methionine and incubated with GST–Rad9 fusion protein. The bound samples were pulled down with glutathione-agarose beads, which were subjected to SDS/PAGE, and gels were exposed to x-ray film. (*Upper*) Pull-down assay. (*Lower Left*) PAGE and exposure of *in vitro* transcribed and translated F1, F2, F3, F4, and FZ fragments (input), shown by asterisks. (*Lower Right*) Immunoblot with anti-GST. (*C*) Assay of colony survival of MEF transfectants after MMS exposure. MEFs transfected with pcDNA expression vector with F1, F2, F3, F4, or FZ cDNA and selected in G418 medium were subjected to colony survival assay, similarly to that shown in Fig. 2*B*. Error bars show standard deviations. (*D*) Cell death after MMS exposure. (*Upper*) Rad9, Rad9-δN (Rad9Ndel), and Bcl2 plasmids were introduced with selection plasmids in F2 transfectants and grown in selection medium for hygromycin resistance. Apoptotic cells were evaluated 48 h after MMS exposure by erythrosine B staining exclusion. (*Lower*) Immunoblot with anti-V5 tag (F2), anti-HA tag (Rad9), anti-HA tag (Rad9Ndel), and anti-Bcl2 antisera.

those *FRAG1* siRNA transfectants at all times after MMS exposure. In sharp contrast, Bax induction was not apparent in control siRNA transfectants in the conditions examined (Fig. 3*B*).

Upon activation by DNA damage-induced or oncogene-induced signaling pathways, phosphorylation of p53 at Ser-15 increases its half-life, accumulation, and tumor suppressing activity (21). Phosphorylation of p53 at Ser-15 leads to reduced interaction of p53 with its negative regulator, the oncoprotein Mdm2, and impairs the ability of Mdm2 to inhibit p53-dependent transactivation (21). Our analysis of two independent Frag1 siRNA transfectants showed that phosphorylation of p53 at Ser-15 was induced in cells after MMS exposure and at 4 (Fig. 3*B*, #406) and 8 h (Fig. 3*B*, #403 and #406) without MMS. In control siRNA transfectants, phosphorylation of p53 at Ser-15 was induced in cells after, but not before, exposure to MMS, showing that, even without MMS, the reduction of Frag1 can stimulate Bax induction in synchronized cells (at 4 or 8 h), emphasizing that reduction of Frag1 sensitizes cells to genotoxic response. Alteration of Mdm2 expression was less apparent. Taken together with the observation by microscopy that cytochrome *c* was released from mitochondria when Frag1 expression was inhibited by siRNA or when cells were exposed to MMS (Fig. 8*C*), it is suggested that reduction of Frag1 may be required for sensitizing cells to DNA damage and activating Bax-related cell death.

p53 translocates to mitochondria, where it directly induces Bax activation and cytochrome *c* release upon DNA damage (22). To determine whether p53 is involved in the induction of Bax expression in our siRNA transfectants, Trp-53-deficient MEFs were analyzed. Results of siRNA Frag1 inhibition showed that Bax was induced in Trp-53$^{+/-}$ and Trp-53$^{-/-}$ transfectants of MEFs and phosphorylation of p53 at Ser-15 was increased in Trp-53$^{+/-}$ transfectants after exposure to MMS, suggesting that Bax was activated regardless of p53 status and that p53 is dispensable for Bax induction in the Frag1 replication stress pathway (Fig. 8*B*). Recently, two p53 homologues have been identified, p73 and p63, that have high amino acid identity, suggesting shared function (23). Indeed, like p53, p73 can trigger several promoters, including Bax and p21 promoters, and is able to trigger cell death in response to the DNA damage. Introduction of p73 oligo siRNA into Frag1 siRNA vector transfectants of Trp-53$^{-/-}$, reduced Bax induction (data not shown), suggesting a role for p73 in the stimulation of the Frag1—Bax pathway.

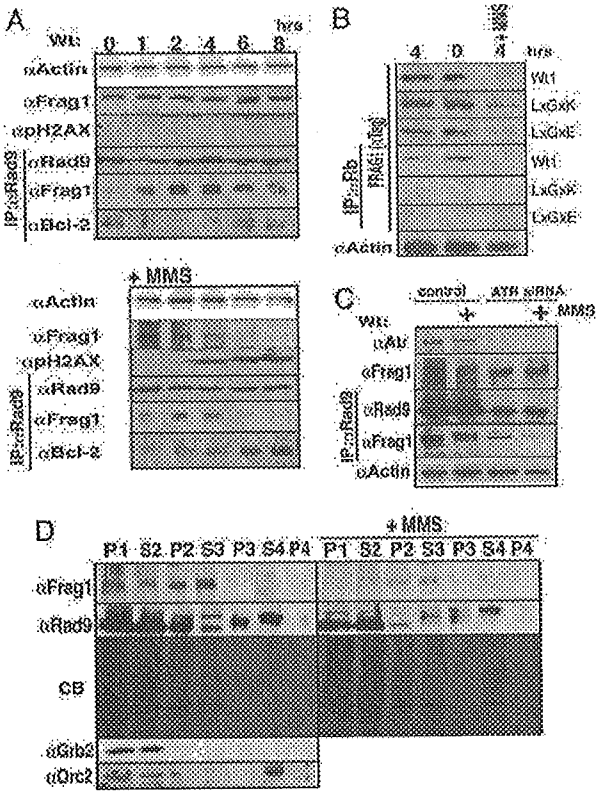

Fig. 5. Frag1 involvement in the DNA damage response. (*A*) Synchronized MEFs were cultured in growth medium with or without MMS (0.01%) for the indicated times, and cellular protein was extracted. Protein expression was studied by immunoblot with the indicated antibodies before and after immunoprecipitation (IP) with Rad9 antibody. (*B*) LxGxK, LxGxE, or wild-type (Wt) Frag1 transfectants that were synchronized at G_1 were released from G_1 in thymidine-free medium with or without MMS (0.01%) as indicated and subjected to immunoblot with anti-V5 (tag) or anti-actin antibody before and after immunoprecipitation with Rb antibody. (*C*) MEFs were transfected with Atr siRNA. A day after transfection, cells were cultured with or without MMS (0.01%) for 4 h, and protein lysates were immunoprecipitated and immunoblotted as indicated. (*D*) Subcellular localization of Frag1 and Rad9 after MMS treatment. Cellular components were fractionated from MEFs before and after exposure to MMS and subjected to immunoblot. Immunoblot with antibodies against Grb2 and Orc2, membranous and chromatin-bound proteins, are shown as controls. P1, whole-cell pellet; S2, cytosol and nucleosol; P2, detergent-insoluble nuclei; S3, DNase I-extracted nuclei; P3, DNase I-resistant fraction; S4, containing chromatin; P4, nuclear matrix. CB, Coomassie brilliant blue staining.

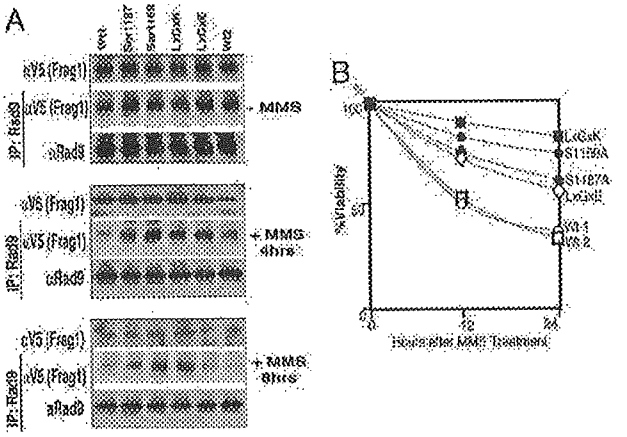

Fig. 6. The Frag1 response to DNA damage. (*A*) Association of Frag1 and Rad9 in response to DNA damage. Wild-type (Wt) and Frag1 mutant MEF transfectants synchronized at G_1 were released from G_1 in thymidine-free medium with 0.01% MMS for 4 or 8 h. Cellular lysates were extracted and subjected to immunoblot with anti-V5 (tag) or anti-actin antibody before and after immunoprecipitation (IP) with Rb antibody. (*B*) Viability of cells expressing wild-type and Frag1 mutants after MMS exposure. Wild-type and Frag1 mutant-expressing MEFs were cultured in medium with 0.01% MMS for the indicated times, and apoptotic cells were evaluated by erythrosine B staining exclusion.

Frag1 Associates with Rad9 and Is Involved in the Bcl2 Pathway. It was shown that proapoptotic Bax can form heterodimers with antiapoptotic Bcl2 in cells (24), which prevents Bax conformational changes required for apoptosis induction (10). Activated Bax proteins oligomerize and are stabilized in the mitochondrial membrane and induce cytochrome *c* release, an important process for the induction of cell death (10). After DNA damage, Rad9 plays a role in induction of apoptosis by associating with antiapoptotic Bcl2, which results in the inhibition of Bcl2 function (9). To investigate the Frag1 signal pathway, we have used coimmunoprecipitation analyses (Fig. 9*A*, which is published as supporting information on the PNAS web site) to define Frag1 associations with partner proteins involved in responses to replicative stress. Immunoblots probed with anti-Frag1 after immunoprecipitation with anti-Rad9 indicated their association in growing cells. Aphidicolin or MMS exposure resulted in reduced Frag1 expression and concomitant reduction of the association with Rad9. Conversely, an increase of Rad9 association with Bcl2 was observed after genotoxic stress (Fig. 4*A*). *In vitro* pull-down assay using recombinant GST–Rad9 fusion protein detected association with *in vitro* transcribed–translated Frag1-F2 fragment, corresponding to the RFC homologous region. Other Frag1 fragments did not associate with Rad9 (Figs. 1*C* and 4*B*), suggesting that the F2 fragment binds Rad9 and regulates apoptosis induction.

Colony formation assays of MEF transfectants expressing specific Frag1 peptides indicated that more colonies formed after F2 expression compared with other Frag1 peptides after genotoxic stress (Fig. 4*C*), suggesting that the F2 region of Frag1 functions to regulate apoptosis by interacting with Rad9. The stable F2 transfectants, in which MMS-induced apoptosis was inhibited, were transfected with Rad9 and selected for hygromycin resistance (Fig. 4*D Upper*, compare F2 and C). Overexpression of Rad9 in the F2 expressors caused an increase in apoptosis (Fig. 4*D*, +RAD9). Usage of Rad9-δN, which is defective in Bcl2 association (9), inhibited apoptosis (Fig. 4*D*, +Rad9Ndel). Furthermore, introduction of antiapoptotic Bcl2 into F2 transfectants resulted in profound inhibition of apoptosis (+Bcl2). Confocal microscopy showed that in F2 transfectants release of cytochrome *c* after exposure to MMS was inhibited (Fig. 9*B*). Results of these experiments strongly suggest that Frag1 modulates Rad9 association with Bcl2 and thereby induces DNA damage-induced apoptosis.

Atr Regulates Frag1–Rad9 Association and the Release of Rad9 from Frag1 in S Phase. To further define Frag1 function, we examined the cell cycle-dependence of Frag1 association with Rad9 in synchronized cells exposed to MMS. Association of Frag1 with Rad9 was weak in synchronized G_1 cells and increased in strength during progression into S phase. After exposure to MMS, the Frag1–Rad9 association was reduced, leading to an increase of Rad9–Bcl2 association (Fig. 5*A*). The data are consistent with the conclusion that Frag1 is involved in sensitizing Rad9 to genotoxic stress during S phase through their association. Confocal microscopic observation indicated that Frag1 and Atr are colocalized 8–12 h after exposure to MMS, whereas Frag1 seems to form foci before Atr focus formation (Fig. 10, which is published as supporting infor-

mation on the PNAS web site), suggesting a role for Frag1 in the Rad9 pathway via Atr response to DNA damage.

To study further the involvement suggested by the Frag1 motif search (Fig. 1*C*) of Atr and Rb in the Frag1–Rad9 pathway, we prepared wild-type and mutant human Frag1 expression vectors by substituting the putative Atr phosphorylation sites, Ser-1169 and Ser-1187 with Ala residues, and the Rb-binding site, LxCxE-1432 with LxGxK-1432 or LxGxE-1432. Transfected wild-type Frag1, but not LxGxE and LxGxK mutants, associated with Rb, as was more apparent in synchronized G_1 than S phase cells (Fig. 5*B*). After MMS, wild-type Frag1 expression was undetectable, whereas LxGxK, and to a lesser extent LxGxE, mutant proteins were detectable. The Frag1–Rb association was undetectable in wild type and two Rb-site mutants after MMS. In summary, it is suggested that Frag1 might play a role in pre-sensitizing cells to genotoxic stress during replication, i.e., in S phase, whereas Frag1 predominantly associates with Rb in G_1 phase.

To examine the role of Atr, endogenous Atr was inhibited by siRNA (Fig. 5*C*). Whereas MMS damage reduced endogenous Frag1 in control cells, reduction of Atr inhibited the down-regulation of endogenous Frag1 in response to DNA damage. Immunoprecipitation showed that, in response to MMS exposure, inhibition of Atr markedly reduced the association of Rad9 with Frag1, a reduction in siRNA ATR-treated cells that was more appreciable than in control cells. Thus, Atr stimulated two separable events: association of Rad9 with Frag1 and down-regulation of Frag1 in response to DNA damage.

Cellular components before and after MMS exposure were fractionated, and proteins were analyzed by immunoblot to study the translocation of Rad9 in response to DNA damage (Fig. 5*D*). After exposure to MMS, the amount of Rad9 in detergent-insoluble nuclei (P2) was significantly reduced, and the proportion of slow mobility Rad9 was increased in DNase I-extracted nuclei (S3), whereas reduction but not translocation of Frag1 was detected, suggesting that a predominant fraction of Rad9 translocated from chromatin to soluble fraction. These results suggest that Frag1 has a role in loading activated Rad9 onto damaged chromatin and stimulating its translocation.

To determine whether phosphorylation and Rb-binding of Frag1 are involved in the association and release of Rad9 (Fig. 6*A*), stable transfectants expressing Frag1 or Frag1 mutants were exposed to MMS, and protein lysates were analyzed by immunoblot. Association of Frag1 with Rad9 was reduced 4 and 8 h after cells were released from G_1 block and exposed to MMS; however, the reduction was inhibited in the Ser-1169A and LxGxK mutants and, to a lesser extent, in Ser-1187A and LxGxE mutants, suggesting that Atr phosphorylation stimulates the dissociation of Rad9 and that Rb binding is also involved, directly or indirectly, in Rad9 activation. The evaluation of apoptotic cells showed that the mutants, especially Ser-1169A and LxGxK, had DNA damage-resistant phenotypes compared with wild-type transfectants (Fig. 6*B*), emphasizing the importance of the Frag1–Rad9 association to apoptosis induction. We finally assessed cotransfectants with Frag1 and wild-type or kinase-dead ATR. Immunoblot analysis showed that, after MMS exposure, down-regulation of Frag1 was inhibited by kinase-dead ATR but not by wild-type ATR (data not shown), supporting the conclusion that phosphorylation by Atr plays a role in the Frag1–Rad9-regulated DNA damage response.

As for a mechanism, our data showed that Frag1 amino acids Ser-1169 and Ser-1187 play critical roles in the regulation of Rad9 release and cell death in response to DNA damage. Ser-1169 and Ser-1187 are putative phosphorylation sites for Atr, which is a sensor of stalled or collapsed replication forks at mid-S phase checkpoint (19). Overexpression of a Rad9-associated Frag1 polypeptide inhibited Bcl2 family-mediated apoptosis, suggesting that Frag1 functions as a platform for loading Rad9 to damaged lesions. As shown in the present study of *ATR* siRNA, after genotoxin exposure, reduction of Atr inhibited the down-regulation of endogenous Frag1 and markedly reduced association of Rad9 with Frag1, suggesting that the loading of Rad9 onto damaged chromatin by Frag1 may require Atr and that Atr could down-regulate Frag1 through phosphorylation sites Ser-1169 and Ser-1187. As for the activation of Rad9, earlier studies showed several mechanisms for recruiting Rad9 to damaged lesions, including Abl-mediated phosphorylation of Rad9, which induced binding of Rad9 to antiapototic BclxL (25); PKCδ phosphorylation of Rad9 after genotoxin exposure (26); and MEC1 and TEL1 of budding yeast, homologues of Atr and Atm, which regulate Rad9 hyperphosphorylation (27). Thus, Atr, in concert with those molecules, can play a direct or indirect role in recruiting Rad9 onto Frag1. Full execution of the steps could lead to the stimulation of the Rad9–Bcl2 cell death pathway. We propose a schema in which each step participates in sensing damage, activating checkpoint, and execution of apoptosis; the multisteps may compose the machinery for the pathway, which determines the fate of cells with perturbations in DNA replication progression, i.e., whether the DNA damage is compatible with cell survival or requires elimination by apoptosis (Fig. 11, which is published as supporting information on the PNAS web site).

We thank Drs. Stuart Schreiber and Karlene Cimprich for kindly providing the plasmids pBJF-ATRwt and pBJF-ATRkd, Drs. Yutaka Eguchi and Yoshihide Tsujimoto for kindly providing pCAGGS-hbcl-2, and Dr. Hong Gang Wang for HA-Rad9 and Flag-Rad9-δN. This work was supported in part by research funds from the High-Tech Research Center Project of the Ministry of Education, Culture, Sports, Science and Technology of Japan, the Mochida Memorial Foundation, and the Cell Science Research Foundation.

1. Rothstein, R., Michel, B. & Gangloff, S. (2000) *Genes Dev.* **14,** 1–10.
2. Bakkenist, C. J. & Kastan, M. B. (2004) *Cell* **118,** 9–17.
3. Levitt, N. C. & Hickson, I. D. (2002) *Trends Mol. Med.* **8,** 179–186.
4. Parrilla-Castellar, E. R., Arlander, S. J. & Karnitz, L. (2004) *DNA Repair* **3,** 1009–1014.
5. Kaina, B. (2003) *Biochem. Pharmacol.* **66,** 1547–1554.
6. Dang, T., Bao, S. & Wang, X. F. (2005) *Genes Cells* **10,** 287–295.
7. Hang, H. & Lieberman, H. B. (2000) *Genomics* **65,** 24–33.
8. Zou, L., Cortez, D. & Elledge, S. J. (2002) *Genes Dev.* **16,** 198–208.
9. Komatsu, K., Miyashita, T., Hang, H., Hopkins, K. M., Zheng, W., Cuddeback, S., Yamada, M., Lieberman, H. B. & Wang, H. G. (2000) *Nat. Cell Biol.* **2,** 1–6.
10. Kirkin, V., Joos, S. & Zornig, M. (2004) *Biochim. Biophys. Acta* **1644,** 229–249.
11. Bellaoui, M., Chang, M., Ou, J., Xu, H., Boone, C. & Brown, G. W. (2003) *EMBO J.* **22,** 4304–4313.
12. Ben-Aroya, S., Koren, A., Liefshitz, B., Steinlauf, R. & Kupiec, M. (2003) *Proc. Natl. Acad. Sci. USA* **100,** 9906–9911.
13. Kanellis, P., Agyei, R. & Durocher, D. (2003) *Curr. Biol.* **13,** 1583–1595.
14. Smolikov, S., Mazor, Y. & Krauskopf, A. (2004) *Proc. Natl. Acad. Sci. USA* **101,** 1656–1661.
15. Merrick, C. J., Jackson, D. & Diffley, J. F. (2004) *J. Biol. Chem.* **279,** 20067–20075.
16. Montes de Oca, R., Andreassen, P. R., Margossian, S. P., Gregory, R. C., Taniguchi, T., Wang, X., Houghtaling, S., Grompe, M. & D'Andrea, A. D. (2005) *Blood* **105,** 1003–1009.
17. Bell, S. P. & Dutta, A. (2002) *Annu. Rev. Biochem.* **71,** 333–374.
18. O'Neill, T., Dwyer, A. J., Ziv, Y., Chan, D. W., Lees-Miller, S. P., Abraham, R. H., Lai, J. H., Hill, D., Shiloh, Y., Cantley, L. C., *et al.* (2000) *J. Biol. Chem.* **275,** 22719–22727.
19. Abraham, R. T. (2001) *Genes Dev.* **15,** 2177–2196.
20. Pennaneach, V., Salles-Passador, I., Munshi, A., Brickner, H., Regazzoni, K., Dick, F., Dyson, N., Chen, T. T., Wang, J. Y., Fotedar, R., *et al.* (2001) *Mol. Cell.* **7,** 715–727.
21. Shieh, S. Y., Ikeda, M., Taya, Y. & Prives, C. (1997) *Cell* **91,** 325–334.
22. Chipuk, J. E., Kuwana, T., Bouchier-Hayes, L., Droin, N. M., Newmeyer, D. D., Schuler, M. & Green, D. R. (2004) *Science* **303,** 1010–1014.
23. De Laurenzi, V. & Melino, G. (2000) *Ann. N.Y. Acad. Sci.* **926,** 90–100.
24. Oltvai, Z. N., Milliman, C. L. & Korsmeyer, S. J. (1993) *Cell* **74,** 609–619.
25. Yoshida, K., Komatsu, K., Wang, H. G. & Kufe, D. (2002) *Mol. Cell. Biol.* **22,** 3292–3300.
26. Yoshida, K., Wang, H. G., Miki, Y. & Kufe, D. (2003) *EMBO J.* **22,** 1431–1441.
27. Vialard, J. E., Gilbert, C. S., Green, C. M. & Lowndes, N. F. (1998) *EMBO J.* **17,** 5679–5688.

Global Analysis of Altered Gene Expressions during the Process of Esophageal Squamous Cell Carcinogenesis in the Rat: A Study Combined with a Laser Microdissection and a cDNA Microarray

Koujiro Nishida,[1] Shinji Mine,[1,2] Tohru Utsunomiya,[1] Hiroshi Inoue,[1] Masahiro Okamoto,[1] Harushi Udagawa,[2] Taizo Hanai,[3] and Masaki Mori[1]

[1]Department of Surgery Medical Institute of Bioregulation, Kyushu University, Tsurumihara, Beppu, Japan; [2]Department of Digestive Surgery, Toranomon Hospital and Okinaka Memorial Institute for Medical Research, Toranomon, Minato-ku, Tokyo, Japan; and [3]Laboratory for Bioinformatics, Graduate School of Systems Life Sciences, Kyushu University, Hakozaki, Higashi-ku, Fukuoka, Japan

Abstract

The genetic alterations that occur during esophageal tumorigenesis have yet to be determined. We previously established a Wister rat carcinogenesis model of esophageal squamous cell carcinoma. To understand more about the molecular mechanisms during carcinogenesis, we produced esophageal neoplastic lesions by administering *N*-amyl-*N*-methylnitrosamine and 12-*O*-tetradecanoylphorbol-13-acetate to rats. We used laser microdissection to specifically isolate the cells from the normal epithelium, papilloma, dysplasia, and invasive carcinoma. Using a cDNA microarray representing 14,815 clones, we then analyzed the gene expression profiles for each esophageal lesion. The number of differentially expressed genes compared with the normal control dramatically increased in a step-by-step fashion from normal epithelium (1,151 ± 119 genes) to papilloma (1,899 ± 543 genes), dysplasia (1,991 ± 193 genes), and invasive carcinoma (2,756 ± 87 genes). A hierarchical clustering analysis showed that the three stages of normal epithelium, dysplasia (papilloma), and invasive carcinoma could be clearly classified, whereas the gene expression patterns of papilloma and dysplasia were indistinguishable. Using the Fisher criterion, we also identified 50 genes whose expression level had either significantly increased or decreased in a step-by-step manner from the normal epithelium to dysplasia and then finally to invasive carcinoma. Many of these genes were not previously known to be associated with esophageal carcinogenesis. The present findings in our rat model thus seem to provide us with a better understanding of the molecular alterations that occur during esophageal carcinogenesis and hopefully will also help lead to the development of novel diagnostic and therapeutic targets. (Cancer Res 2005; 65(2): 401-9)

Introduction

We previously established a rat carcinogenesis model of esophageal squamous cell carcinoma (ESCC) by administering *N*-amyl-*N*-methylnitrosamine (AMN) as an initiator, and 12-*O*-tetradecanoylphorbol-13-acetate (TPA, a phorbol diester) as a promoter. In this model, papilloma, dysplasia, and invasive carcinoma were successfully developed by the combined administration of AMN and TPA. Our findings suggest this model to be useful to both investigate and characterize the malignant lesions occurring in the esophagus (1). Since publishing our earlier findings, our knowledge of molecular pathogenesis during cancer development has dramatically improved. For example, the process of colon carcinogenesis has been well documented as an adenoma-carcinoma sequence. In this theoretical model, multistep genetic alterations were clarified, such as the deletion and mutation of the APC, the mutation of the K-*ras*, and abnormalities in the 17th and 18th chromosomes (2, 3). Regarding esophageal carcinogenesis, an increased expression of cyclin D1 was observed not only in esophageal carcinoma but also in precancerous dysplastic lesions (4, 5). An accumulation of p53 protein was also found in the cell nuclei of precancerous and cancerous lesions of the esophagus (6). Although such genetic alterations are possibly early events of esophageal carcinogenesis, there is still a need to clarify these processes at a molecular level. The recent development of large-scale gene expression profiling by DNA microarrays now allows for the concurrent analysis of thousands of genes, and the molecular pathways possibly involved in human ESCC tissues (7–10) and esophageal cancer cell lines (11–13) have also been reported. Most of the former microarray studies compared the gene expression profiles between ESCC tissues and matched normal tissues, however, few studies have investigated the expressional changes during multistep carcinogenesis (7). Furthermore, all of these data derived from bulk tumor tissues might not adequately reflect the cell-type specific expression profiles, because ESCC contain various types of cells, such as mesenchymal cells and inflammatory cells. Indeed, the proportions of neoplastic cells in such tissue samples are quite different from one case to another. On the other hand, several animal studies have shown the molecular changes during tumorigenesis by a technique of DNA microarray (14–18). Again, these studies examined the gene expression patterns of bulk tumor tissues. Taking all of these issues into account, we reproduced our rat carcinogenesis model and prepared purified proportions of the cells by means of laser microdissection (LMD). To the best of our knowledge, this is the first study to identify the global gene expression profiles during the process of multistep carcinogenesis by integrating the technologies combined with LMD and cDNA microrarray. The present findings in our rat model would greatly help us to understand the molecular alterations during esophageal carcinogenesis as well as also help us to identify novel diagnostic and therapeutic targets.

Materials and Methods

Animals and Chemicals. Wistar rats, 4-week-old males, obtained from Nihon Seibutsu Zairyo Center, Tokyo, Japan, were allowed free access to a

Requests for reprints: Masaki Mori, Department of Molecular and Surgical Oncology, Medical Institute of Bioregulation, Kyushu University, Tsurumihara 4546, Beppu, 874-0838, Japan. Phone: 81-977-27-1650; Fax: 81-977-27-1651; E-mail: mmori@tsuruni.beppu.kyushu-u.ac.jp.

standard laboratory chow diet (Oriental Koubo Co., Tokyo, Japan) and water for 7 days before commencing the experiments. All the experimental animals used in this study received humane care according to the guidelines outlined in the Guide for the Care and Use of Laboratory Animals by the National Academy of Science (NIH publication no. 86-23, revised 1985). As described previously (1), AMN was dissolved in tap water at a final concentration of 0.003% and was given to these rats *ad libitum*. TPA was dissolved in pure acetone to a concentration of 0.1 mg/mL and was added to the drinking water to reach a final concentration of 0.1 g/mL. This diluted solution was freshly prepared every 2 days.

Experimental Groups. The 24 rats were divided into four groups with the following treatment regimens: group A, AMN for 4 weeks; group B, AMN for 4 weeks followed by TPA for 8 weeks; group C, AMN for 12 weeks followed by TPA for 4 weeks; group D, untreated controls received neither AMN nor TPA (Table 1).

Tissue Sampling. All rats were observed for 20 weeks from the beginning of treatment and were sacrificed at the end of the experiment. The esophagus from every rat was cut out and the tissue blocks from the normal esophageal epithelium, papilloma, dysplasia, and carcinoma were obtained. Each block was cut into two pieces, with one half being used for the pathologic diagnosis, and the other half being used for the molecular analysis. The latter halves were immediately embedded in a Tissue Tek OCT compound medium (Sakura, Tokyo, Japan) and kept frozen at −80°C until they were microdissected.

Histologic Examination. The pathologic diagnosis was done with H&E staining. Papilloma was characterized by exophytic tumors of squamous cell type with hyperkeratinization. The basal layer of the papilloma was well preserved, and the cellular and nuclear atypism was slight (19, 20). Dysplasia included amorphous cells extending from the basal cell layer, except for a thin superficial layer. If all layers of the epithelium showed dysplastic change, the lesions were defined as carcinoma *in situ*. When invasion was beneath the basement membrane and severe cellular atypism was present, the lesion was described as invasive carcinoma (21). Because it was difficult to clearly distinguish carcinoma *in situ* from severe dysplasia, we decided to exclude carcinoma *in situ* from this study.

Laser Microdissection. For LMD, the Application Solutions Laser Microdissection System (Leica Microsystems, Wetzlar, Germany) was used. Serial 8-μm-thick sections were prepared with a cryostat and were mounted onto a foil-coated glass slide, 90 FOIL-SL25 (Leica Microsystems). The sections were then fixed in 100% ethanol for 3 minutes and stained with H&E staining protocol to maintain the morphologic quality required for accurate microdissection. After careful drying, the sections were laser microdissected according to the manufacturer's instructions (Leica Microsystems).

RNA Extraction, T7-Based RNA Amplification, and Quality Check of Amplified RNAs. Total RNAs were extracted from each sample of laser microdissected cells into 350 μL of buffer RLT (Qiagen, Hilden, Germany) added β-mercaptoethanol to a concentration of 1%. Next, total RNAs were purified with the RNeasy Mini Kit (Qiagen) according to the manufacturer's protocol. All of the total RNAs were subjected to two rounds of T7-based RNA amplification as described previously (22). In brief, whole total RNA was reverse-transcribed by using oligo-dT T7 primer containing the T7 RNA polymerase binding site (5′-AAACGACGGCCAGTGAATTGTAATACGACTCACTATAGGCGCT15-3′; refs. 23, 24). Next, second strand cDNA synthesis was done with RNase H, *Escherichia coli* DNA polymerase I and T4 DNA polymerase (TaKaRa Shuzo, Shiga, Japan). The cDNA was then purified and transcribed with MEGA script T7 Transcription Kits (Ambion, Inc., Austin, TX). The purity and concentration of amplified RNA (aRNA) were determined by Agilent 2100 bioanalyzer (Agilent Technologies, Palo Alto, CA).

cDNA Microarray (Labeling, Hybridization, and Scanning). We used the Rat cDNA Microarray (Agilent Technologies) which contains 14,815 clones with 7,575 annotated genes, 5,769 expressed sequence tag clones, and 1,471 other unnamed clones. A list of genes on this cDNA microarray is available at http://www.agilent.com/chem/genelists. Five hundred nanogram aliquots of each aRNA from the 12 esophageal tissue samples (three samples from each of normal esophageal epithelium, papilloma, dysplasia, and invasive carcinoma) were labeled with Cyanine 5-dUTP (Perkin-Elmer/NEN, Boston, MA), whereas a 500-ng aliquot of aRNA from a mixture of three normal esophageal epithelium were labeled with Cyanine 3-dUTP as control. The labeled probes were then hybridized with the rat cDNA microarray in hybridization buffer (Agilent Technologies) for 17 hours at 65°C. After hybridization, the slides were washed in 0.5× SSC/0.01% SDS for 5 minutes at room temperature and 0.06× SSC for 2 minutes at room temperature (25). The Cy3 and Cy5 fluorescent intensities for each spot were determined by an Agilent DNA Microarray Scanner and then were analyzed by G2566AA Feature Extraction Software vA.6.1.1 (Agilent Technologies), which used the LOWESS (locally weighed linear regression curve fit) normalization method (26).

cDNA Microarray Data Analysis. After subtracting the local and global background signals, the expression values were calculated as the log ratio of the dye-normalized red (Cy 5) and green (Cy 3) channel signals. The data flagged as being of poor quality according to the Agilent data extraction software were removed from the analysis. All data calculated by data extraction software were imported to the Rosetta Luminator system v2.0. (Rosetta Biosoftware, Kirkland, WA). All the intensity data were plotted as a log ratio. Next, a hierarchical clustering analysis was done using the Rosetta Luminator system. The gene expression profiles of three stages, including normal epithelium, dysplasia, and invasive carcinoma were further analyzed and compared. To compute the Fisher criterion, three stages were divided into two patterns of two groups as follows: Pattern 1, a group of normal epithelium and dysplasia versus a group of invasive carcinoma; Pattern 2, a group of normal epithelium versus a group of dysplasia and invasive carcinoma. First, we identified the top 500 genes from each pattern. We then selected the genes common to the top 500 genes (302 up-regulated and 198 down-regulated) in Pattern 1 and those (226 up-regulated and 274 down-regulated) in Pattern 2. The original data will be available at URL of supplemental web site at http://www.mib-beppu.kyushu-u.ac.jp/MIB_res/clin_surg/MA/MA_data.html.

Real-time reverse transcription-PCR Assay. The real-time reverse transcription-PCR (RT-PCR) assay was done using the same aRNA samples

Table 1. Development of papilloma, dysplasia, and invasive carcinoma in the rat esophagus

Group	Treatment	No. rats	Lesion incidence (%)		
			Papilloma	Dysplasia	Carcinoma
A	AMN, 4 wk	6	33	33	0
B	AMN, 4 wk → TPA, 8 wk	6	33	50	17
C	AMN, 12 wk → TPA, 4 wk	6	67	33	83
D	No treatment, control	6	0	0	0

that had served for the microarray analysis. The following primers were used to amplify the genes of interest: Rat matrix metalloproteinase 2 (*Mmp2;* F-TCAAGTTCCCCGGCGATGTC and R-TTGCGGGGAAA-GAAGTTGTAGT), Rat cathepsin H (*Ctsh;* F-GTGCCCAGAACTTCAACAATCAT and R-AACGCGACGGCCTTTTCTG), Rat serine protease (*C1s;* F-GGCCA-GAGGTCCAGCAAGAG and R-GGGGGCAGGAGCAGAAGTATC), Rat DRAL (*Fhl2;* F-GAAGCAGCTATCTGGGCAAC and R-TGGCGTTCCTCAAAAGAGAT). Rat aldehyde dehydrogenase (*Aldh1a1;* F-GGGCAGCGATCTCCTCTCACAT and R-CAAGTCGGCATCTGCAAACACAA). Rat cytochrome *P*4502F4 (*Cyp2f1;* F-GGGGCCCAGGCGTGTGATT and R-TCCGCTCCTCGATGCTTCTTTT). Rat *β-actin* (F-CCTAAGGCCAACCGTGAAAAGATG and R-GTCCCGGCCAGC-CAGGTCCAG) was used as an internal standard.

Statistical Methods. The data were expressed as the means ± SD. We used Student's *t* test and Fisher's exact test to assess differences. These data were analyzed with StatView for Windows version 5.01 (SAS Institute, Inc., Cary, NC), and the findings were considered significant when the $P < 0.05$.

Results

Macroscopic and Histologic Findings during Rat Esophageal Carcinogenesis. The macroscopic findings of each lesion are shown in Fig. 1. A histologic examination confirmed each lesion including papilloma, dysplasia, and invasive carcinoma in our rat model (Fig. 1). The incidences of each lesion among the four groups are summarized in Table 1. Papilloma and dysplasia were observed in groups A, B, and C treated with AMN. Group C exhibited a higher incidence of invasive carcinoma than the other groups. There was no detectable papilloma, dysplasia, or carcinoma in group D treated with neither AMN nor TPA. The histologic features of all esophageal carcinomas were squamous cell origin.

T7-Based RNA Amplification and Quality Check of Amplified RNAs. One of the most important steps in gene expression workflow was the quality assessment of RNA samples to ensure the success of gene expression analysis. The purity and concentration of aRNAs were carefully determined using an Agilent 2100 bioanalyzer (Agilent Technologies). Representative electropherograms of successful RNA amplification from each lesion are shown in Fig. 2. High-quality aRNA run on a bioanalyzer typically has the shape of a hump peak, which means no contamination of rRNA. Two rounds of T7-based RNA amplification yielded 5 to 40 μg of aRNA from each sample, and they were sufficient to perform cDNA microarray (27, 28). We successfully obtained high-quality aRNAs, of which quality were verified with the bioanalyzer, from 12 esophageal tissue samples (three samples each of normal epithelium, papilloma, dysplasia, and invasive carcinoma). All of them were employed for the following cDNA microarray analysis.

cDNA Microarray Data Analysis. All intensity data were plotted as a log ratio with the Rosetta Luminator system (Rosetta Biosoftware). The number of differentially expressed genes remarkably increased during the process of esophageal carcinogenesis (Fig. 3). In the normal epithelium, 1,151 ± 119 clones were determined as differentially expressed genes in comparison with the normal control (mixture of three normal epithelium), indicating a high correlation coefficient ($R = 0.93 \pm 0.03$). In contrast, 1,899 ± 543 clones in papilloma ($R = 0.87 \pm 0.05$) and 1,991 ± 193 clones in dysplasia ($R = 0.87 \pm 0.03$) were determined as differentially expressed genes. Furthermore, invasive carcinoma contained 2,756 ± 87 differentially expressed genes compared with control, showing a significantly lower correlation coefficient ($R = 0.74 \pm 0.02$) compared with those of other three stages ($P < 0.01$). A hierarchical clustering analysis showed that the normal epithelium, papilloma (dysplasia), and invasive carcinoma could be well classified, whereas the gene expression patterns between papilloma and dysplasia were indistinguishable (Fig. 4). To further confirm the integrity of our cDNA microrarray system, we first evaluated the expression levels of three genes, which are generally well known to be cancer related. The results revealed the expression levels of *cyclin D1* (Rat mRNA for *cyclin D1*) and *Mdm2* (mouse *Mdm2* gene) to be elevated in invasive carcinoma following by dysplasia (Fig. 5). *Cyclin D1* was also overexpressed in papilloma. The expression of *APC* (mouse adenomatous polyposis coli) was down-regulated in invasive carcinoma following by dysplasia. These results were well correlated to the previous reports (29–33). We then statistically searched the differentially expressed genes during ESCC progression. Human ESCC develops more frequently from dysplasia than papilloma. We thus analyzed the differentially expressed genes among the following three stages, normal epithelium, dysplasia, and invasive carcinoma. By means of the Fisher criterion (34), we selected 41 up-regulated genes and nine down-regulated genes associated with the process of esophageal carcinogenesis (Table 2*A* and *B*). The gene lists contained the genes encoding for proteases and plasminogen activator receptor and those associated with cell adhesion and cell growth. In addition, some cancer-related

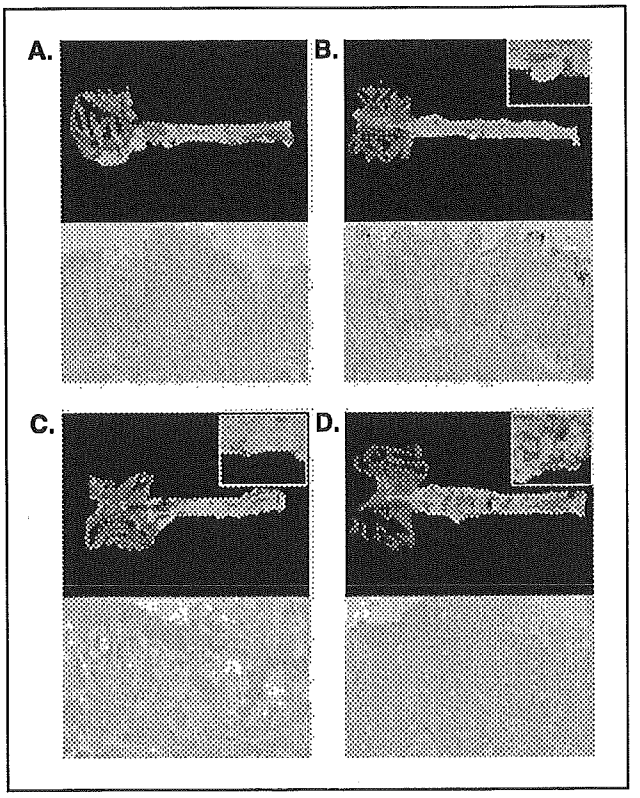

Figure 1. Macroscopic and microscopic findings (H&E staining) of each lesion of the rat esophagus. *A*, normal esophageal epithelium. *B*, papilloma. *C*, dysplasia. *D*, invasive carcinoma. In the microscopic findings, papilloma was characterized by squamous cell type exophytic tumors with hyperkeratinization and their basal layer was well preserved (*B*). Dysplasia included amorphous cells extending from the basal cell layer, except for a thin superficial layer (*C*). The invasion was beneath the basal layer and severe cellular atypism was present (*D*).